Physics of Complex Systems

PHYSICS OF COMPLEX SYSTEMS

CONTENTS

Dear Colleagues,

Welcome to the Physics of Complex Systems journal. Our journal, as the title suggests, interrogates the complexity of the systems placed under the scrutiny of modern physics, be it the Universe or a nanometer-sized quantum dot. The journal is designed to promote scientific advances of university scholars and provide academics, researchers and students alike with an opportunity to share their research findings with peers. The Physics of Complex Systems publishes experimental and theoretical papers in different fields of physics from metals to insulators, from nanostructures to cosmology.

I am deeply grateful to all my colleagues who kindly agreed to be members of the Editorial Board and to share the commitment to make our journal an effective platform for knowledge exchange. The extensive expertise of Russian and international Board members will ensure the highest quality of publications. The Physics of Complex Systems is a peer-reviewed open-access journal with an international team of reviewers. We are doing our best to ensure timely review of all submissions (within two weeks).

Internationalisation of modern science means that research findings need to be effectively disseminated among the world scientific community. To fulfil this mission, the Physics of Complex Systems publishes papers predominantly in English as the international language of scientific communication. Besides, the journal is available online to facilitate access to its papers around the world.

Our primary goal is to create a knowledge exchange platform for institutions of higher education, but we are equally pleased to welcome submissions from other research organisations as well as from international teams of authors. The Board especially encourages submissions from young scholars and graduate students–emerging leaders in various fields of science, technology, and management.

It is our ambition to make the Physics of Complex Systems one of the most reputable and high-profile physics journals and we thank all those–the Editorial Board members as well as our contributors and reviewers–who joined us in our efforts to achieve this goal. Our immediate priority is to ensure that the Physics of Complex Systems is indexed in the Scopus and Web of Science databases.

We are looking forward to receiving your manuscripts.

Sincerely yours,
Alexander Kolobov
Editor-in-Chief

Characteristic energy loss of electrons in Mg with angle resolution

V. P. Pronin[1], I. I. Khinich[✉1]

[1] Herzen State Pedagogical University of Russia, 48 Moika River Emb., Saint Petersburg 191186, Russia

Authors

Vladimir P. Pronin, ORCID: 0000-0001-9335-9781

Iosif I. Khinich, ORCID: 0000-0002-1745-8742, e-mail: khinitch@gmail.com

Abstract. The article discusses electron energy loss of bulk and surface plasmons in solid polycrystalline Mg films. The experimental study of the electrons' characteristic energy loss is conducted and its results are compared in a wide range of electron incidence angles on the sample (0°–89°), dispersion angles (5°–165°) and electron energies (100–600 eV). Electron wave refraction at the vacuum–solid state interface is considered as one of the factors determining the intensity of surface plasmons.

Keywords: electron spectroscopy, bulk plasmons, surface plasmons, elastic electron scattering, electron wave refraction.

Introduction

Electron energy loss spectroscopy is an effective modern method for analysing near-surface solid state regions and obtaining data on the density of electronic states and plasmon excitations. Spectroscopy identifies special energy spectra features of non-elastically reflected electrons that arise from fixed energy loss of some low-loss electrons (elastic reflected electrons peak, EREP) and, therefore, are observed as separated from the EREP by the value of this loss. The nature of the loss may vary; it is connected with quasiparticle excitation in the solid state (phonons and plasmons), single-particle excitation of valence electrons (intraband and interband transitions), and ionisation of internal atomic levels. Electron energy loss spectroscopy can be carried out in a wide range of electron energies by various experimental methods, achieving the required resolution at very low and very high excitation energies. Most common methods use seed electrons with energies within hundreds of eV. In this energy range surface and bulk plasmons as well as intraband and interband transitions get excited (Iakoubovskii, Mitsuishi, Nakayama, Furuya 2008; Oura, Lifshits, Saranin et al. 2006). Energy resolution around tenths of eV, which does not require additional monochromatisation of the electron beam, is necessary to interpret visible features of the spectrum.

Experimental procedure

The experimental analysis was conducted using a universal electron spectrometer based on the USU-4 ultra-high vacuum set. The spectrometer is fitted with a quasi-spherical condenser which is a two-grid analyser that determines angularly integral parameters of elastically and non-elastically reflected electrons at normal incidence. It is also fitted with a mobile portable electron spectrometer used for studying angularly differential parameters of electrons within incident angles 0°–89° and scattering angles 5°–165°.

Angle-resolved electron energy loss spectroscopy is performed in order to vary the zone of examination by changing incident angles, emergent angles and electron energies, and to reveal changes in electron state density in passing from surface to volume.

In general, plasmons come into sharp focus in substances which meet two requirements simultaneously: (1) there is a fairly isolated (with respect to energy) group of valence electrons; and (2) plasmon energy corresponding to oscillations of electrons in this group is relatively far from the band-to-band transition energies typical for this substance (otherwise, plasmons quickly become damp due to strong plasmon-electron interactions). Mg films meet these criteria; therefore, they were chosen for this study. Features of energy loss spectrum for Mg films may only be determined by excitement of bulk and surface plasmons. Mg films were formed using the method of thermal evaporation on cooled mirrored glass base in vacuum $\sim 10^{-7}$ Pa, so that the surface was rough enough.

Energy loss spectra for Mg were studied in the energy range $E_p = 100 - 600$ eV. They were analysed according to the following procedure. Firstly, an approximation of loss was made within the measured spectra independently of collective mode excitation similar to approximation (Iakoubovskii, Mitsuishi, Nakayama, Furuya 2008). The EREP and peaks related to the excitement of bulk and surface plasmons were approximated with the Gaussian distribution:

$$I_i = A \cdot e^{-\frac{(\Delta E_i - \Delta E)^2}{2\sigma_i^2}}$$

where ΔE_i is the plasmon excitation energy value; σi is the dispersion determined by EREP dispersion (σ_r) and plasmon dispersion (σ_p):

$$2\sigma_i^2 = 2\sigma_r^2 + 2\sigma_P^2$$

Then the loss rates and the EREP rates were defined as areas below the corresponding peaks.

Experimental results

Complex investigation of energy loss spectra including electron energies, their incident angles and angles of emergency from the surface can be carried out based on comparative analysis of results obtained from the following three types of studies: (1) measurement of energy spectra at a fixed angle of emergence depending on the incident angle φ; (2) measurement of energy spectra at a fixed incident angle depending on the angle of emergence α; (3) measurement of energy spectra at fixed incident and emergent angles depending on the energy of primary electrons.

Let us consider the Mg spectra behaviour with changing electron incidence angle (Fig. 1). Bulk plasmon energy is 10.5 eV, which corresponds with the previous research data (Raether 1980). As the incident angle increases and, therefore, the penetration depth of the initial beam into the sample decreases, quick weakening of the bulk loss peak is observed. Fig. 2 shows the dependence of the second type on the incident angle α. According to the spectral analysis, it is possible to conclude that at relatively small incident and emergent angles of electrons the ratio A_{SI}/A_r (where A_{SI} is the intensity of the first surface loss, A_r is the intensity of EREP), to the accuracy of experimental precision that does not exceed approximately 5%, is defined by the following formula (with the assumption of two-part process of the surface loss development):

$$\frac{A_s}{A_r}(\varphi, \alpha) = \frac{B}{\cos\alpha} + \frac{C}{\cos\varphi}$$

which corresponds to the perceptions of dielectric formalism (B is a constant defined by the intensity of primary electron beam; C is defined by the intensity of EREP) (Stern, Ferrell, 1960). However, at reasonably large incident angles $\varphi > 80°$ the surface loss intensity does not change significantly.

The effect discovered may be interpreted by electron wave refraction at the solid state–vacuum interface:

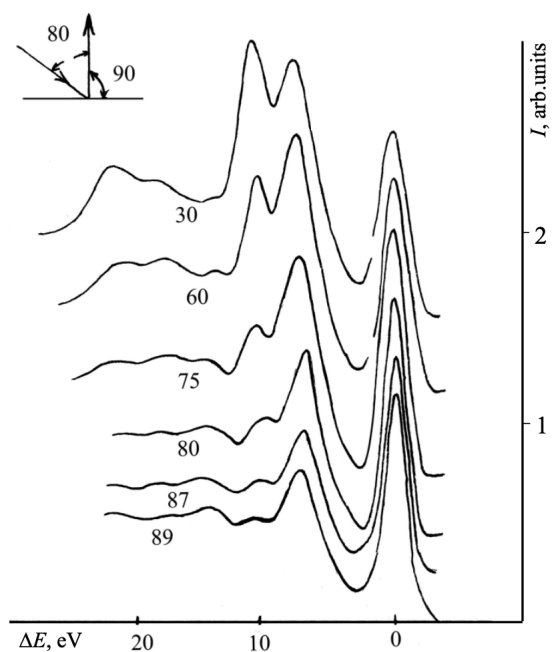$$\frac{\sin\varphi}{\sin\varphi'} = \frac{\sin\alpha}{\sin\alpha'} = \sqrt{\frac{E + eU_0}{E}}$$

Fig. 1. Electron energy loss spectra for Mg. E_p = 200 eV. α = 0°. Incident angles ϕ in degrees are specified near the curves
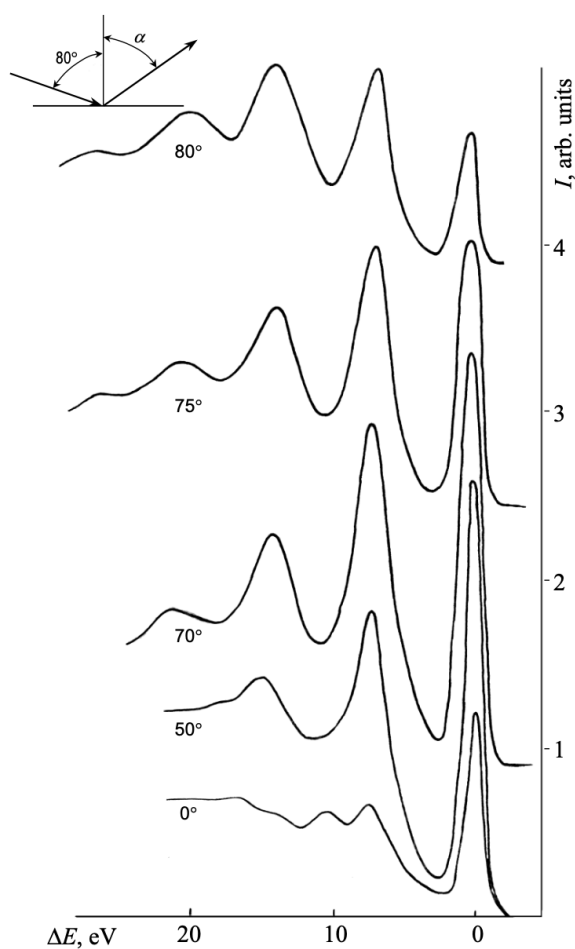
Fig. 2. Electron energy loss spectra for Mg. E_p = 100 eV. ϕ = 80°. Emergent angles α are specified near the curves
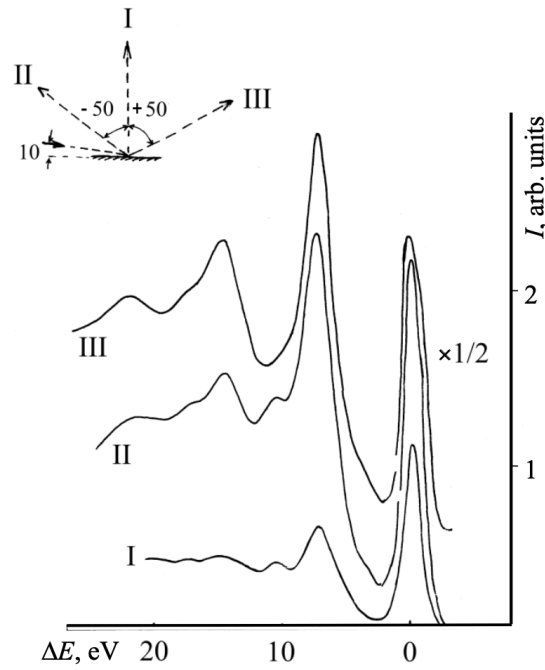
Fig. 3. Electron energy loss spectra for Mg. E_p = 200 eV. ϕ = 80°. Emergent angles: I correspond to 0°; II, III corresponds to 50°

where α' and ϕ' are the inner angles of electron incidence and emergence, U_0 is the effective inner potential of solid state. With increasing incident angle ϕ from 80° to 89° (Fig. 1), the inner incident angle changes from 74° to 79°, which leads to insignificant difference in the electron energy loss spectrum.

Fig. 3 illustrates the comparison of electron energy loss spectra at the electron incidence angle ϕ = 80° at two symmetrical angles of emergence corresponding to very different scattering angles. In this case, the intensity of surface loss peaks at small scattering angles and significantly exceeds those for big scattering angles where bulk plasmon peaks are observable. The result seems to derive from the fact that electrons with small scattering angles elastically reflected once and the electrons that experienced multiple scattering contribute differently to the electron energy loss intensity peaks. The electrons reflected once at small angles from the surface of solids (their contribution is 70–80 % of the total amount of reflected electrons) play the main role in forming the electron energy loss spectrum in the region of small scattering angles. For large angles this contribution is substantially smaller, and the role of electrons emerging from relatively large depths becomes significant as they cause volume loss (bulk plasmon).

Fig. 4 illustrates changes in electron energy loss spectra depending on the changes in incident electron energy. As energy increases and the depth of the primary beam penetration distance grows, the intensity of the bulk loss peak also grows.

Energy dependences $\frac{A_{s1}}{A_r}(E_p)$ corresponding to the experimental data in the entire given interval of energies with relatively small angles ϕ and α are close to the theoretically predicted probability of surface loss that is in accordance with the perceptions of dielectric formalism (van Attekum, Trooster 1979):

$$W_S \sim \frac{1}{E^{1/2}}$$

However, for big incident and emergent angles, the dependence $\frac{A_s}{A_r}(E_p)$ (fig. 5) is different.

This result can be explained by the above-mentioned phenomenon of electromagnetic wave refraction at the solid state–vacuum interface. From this perspective, experimental dependences $\frac{A_s}{A_r}(E)$ may be described as:

$$\frac{A_S}{A_r}(E) = \frac{C}{E^{1/2}} \cdot F(\alpha', \varphi') \tag{1}$$

where α' and ϕ' are inner emergent and incident angles.
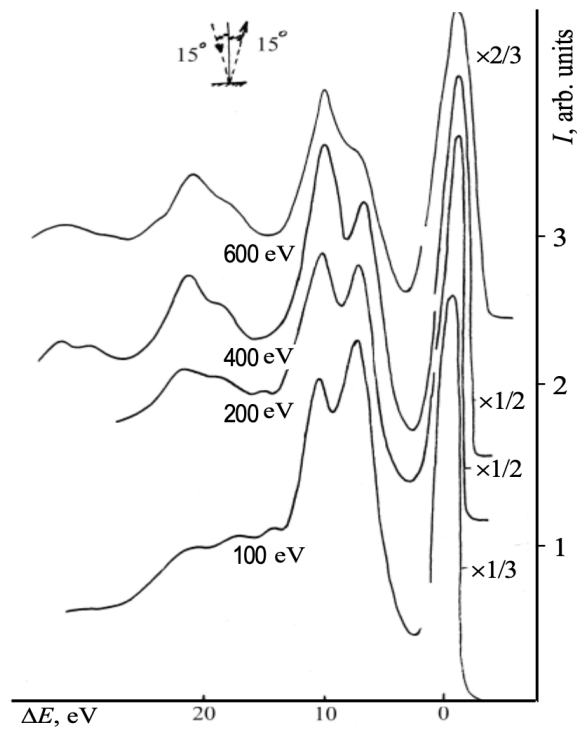
Fig. 4. Electron energy loss spectra for Mg. $\overset{\prime}{\phi} = \alpha = 15°$. Primary electron energies are specified near the curves. The size of elastic reflected electron peaks is reduced in proportion to the figures indicated
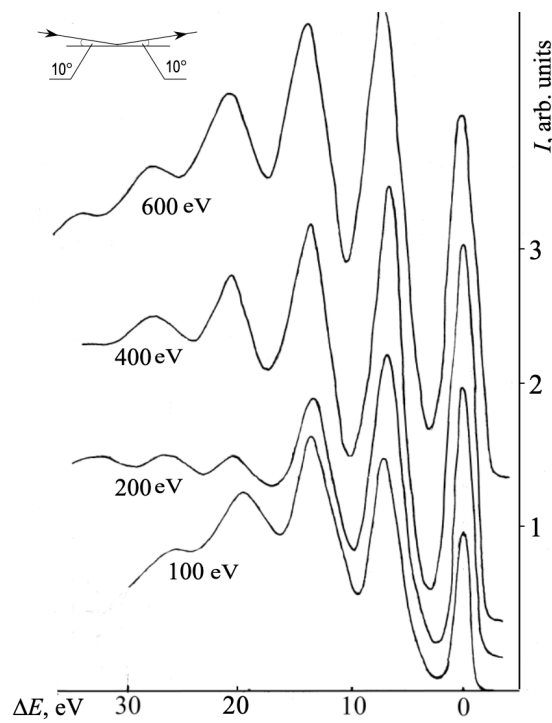
Fig. 5. Electron energy loss spectra for Mg. $\phi = \alpha = 80°$. Primary electron energies are specified near the curves

It appeared that the dependences calculated using the formula (1) correspond with the experimental results (Fig. 6).

Fig. 6. Dependence of ratio of first surface plasmon intensity to EREP intensity from primary electron energy for Mg. $\phi = \alpha = 80°$. The solid curve corresponds to the experiment, points correspond to the calculations.

Conclusion

Detailed investigation of angle-resolved electron energy loss spectra showed that for correct reading of experimental results it is essential to take into account the character of elastic electron scattering and the influence of electron wave refraction at the solid state–vacuum interface.

References

Iakoubovskii, K., Mitsuishi, K., Nakayama, Y., Furuya, K. (2008) Thickness measurements with electron energy loss spectroscopy. *Microscopy Research & Technique*, 71 (8), 626–631. DOI: 10.1002/jemt.20597 (In English)

Oura, K., Lifshits, V. G., Saranin, A. A. et al. (2006) *Vvedeniye v fiziku poverkhnosti [Introduction to surface physics].* Moscow: Nauka Publ., 490 p. (In Russian)

Raether, H. (1980) Surface excitations. In: H. Raether. *Excitation of plasmons and interband transitions by electrons.* Berlin; Heidelberg: Springer, 116–171. DOI: 10.1007/BFb0045962 (In English)

Stern, E. A., Ferrell, R. A. (1960) Surface plasma oscillations of a degenerate electron gas. *Physical Review*, 120 (1), 130–136. DOI: 10.1103/PhysRev.120.130 (In English)

van Attekum, P. M. Th. M., Trooster, J. M. (1979) Bulk- and surface-plasmon-loss intensities in photoelectron, Auger, and electron-energy-loss spectra of Mg metal. *Physical Review B*, 20 (6), 2335–2340. DOI: 10.1103/PhysRevB.20.2335 (In English)

Dye-sensitized photoprocesses in "silver stearate – silver bromide" system

M. A. Goryaev[1], A. P. Smirnov[✉1]

[1] Herzen State Pedagogical University of Russia, 48 Moika River Emb., Saint Petersburg 191186, Russia

Abstract. The article provides a comprehensive description of spectral sensitization of photothermographic materials, showing a significant influence of dye molecules localized on the surface of silver stearate on the spectral sensitization process of photothermographic materials. It demonstrates that silver stearate effectively transfers dye molecules luminescence to the silver bromide microcrystal with a lightguide mechanism.

Keywords: spectral sensitization, photothermographic materials, luminescence, silver stearate, silver bromide, Rhodamine 6 G.

Introduction

In addition to CCD and CMOS sensors, the photothermographic materials based on silver halide and silver salts of fatty acids (in particular silver stearate) compositions are used quite widely to record optical images (Goryaev 1991; Morgan 1993; Sahyun 1998). When preparing such photosensitive composition, silver bromide is synthesized on the surface of silver stearate (Goryaev 1994a; 2013). Spectral sensitization process can be achieved by adding various dye-sensitizers into this photothermographic composition. Therefore, it is possible to attain photosensitivity of such compositions in any optical spectral range (Goryaev 2011; 2013).

Results and discussion

Dye molecules precipitate both on the surface of silver stearate and on the surface of silver bromide when this dye is adsorbed into photothermographic compositions. Silver stearate is a transparent dielectric in visible range (Goryaev, Smirnov 2012). Dyes adsorbed on different dielectric surfaces radiate with luminescence quantum yield of a few dozen per cent (Goryaev 2013). Therefore, a large quantity of luminescence light transmits through the silver stearate particle and hits the microcrystal of silver bromide. The luminescence of the dye adsorbed on silver stearate was investigated with the use of the "white standard" dilution method (Goryaev 1980; Goryaev, Smirnov 2015). Figure 1 shows the ratio of the luminescence technical yield of Rhodamine 6G adsorbed on the surface of silver stearate to the degree of dilution by "white standard" (magnesium oxide). The technical quantum yield increases at first and then becomes constant with decreasing concentration of the dyed sample in the magnesium oxide powder. The constant value of the technical yield is the true luminescence quantum yield of the adsorbed dye (Goryaev 1980).

In many sensitizing dyes, luminescence and absorption spectra strongly overlap (Goryaev 1981). Figure 2 shows the absorption and luminescence spectra of Rhodamine 6 G adsorbed on silver stearate.

Since absorption and luminescence spectra strongly overlap, the luminescence radiated by the dye molecules adsorbed on silver stearate is effectively absorbed by the dye adsorbed on the silver bromide surface. Therefore, luminescence light induces the photophysical and photochemical processes required for photographic process in silver bromide. The dye molecules adsorbed on silver bromide absorb luminescence light and become able to transfer energy directly to silver bromide according to the theory of the non-radiative resonant inductive energy transfer (Akimov, Cherkasov, Cherkashin 1980; Ermolaev, Sveshnikova, Bodunov 1996).

Consequently, the dye molecules adsorbed on silver stearate, as well as on silver bromide, exert significant influence on the spectral sensitization process, where silver stearate ensures sufficiently effective transmission of energy from dye molecules to the sensitivity centers of silver bromide. This is confirmed by the fact that the optimal concentration of dye in photothermographic compositions is substantially higher than in classic silver halide emulsions (Goryaev 2011; Goryaev, Kolesova, Timohina et al. 1992).

Efficient spectral sensitization has been observed (Goryaev, Kolesova, Timohina et al. 1992) in the compositions where silver bromide was synthesized directly on the surface of silver stearate. In this case, the optimal concentration of silver halide in relation to silver stearate is 10 mol%. The ratio for the volume concentration of silver bromide microcrystals is as follows:

$$c_{vol} = \frac{cMd'}{M'd} \tag{1}$$

where c is the molar concentration of silver halide, M and M' are the molecular masses of silver bromide and silver stearate respectively, d and d' are the density of silver bromide and silver stearate respectively. In case of $M = 187.8$, $M' = 391.3$, $d = 6.47$, $d' = 1.40$ and $c = 0.1$, c_{vol} is 0.0104. Further assuming that the particles of silver halide and silver stearate are cubes, it is possible to estimate the ratio of the silver stearate surface area s' to silver halide s:

$$\frac{s'}{s} = 1.2 \ (c_{vol})^{-\frac{2}{3}} - 0.2 \tag{2}$$

Given this assumption and $c_{vol} = 0.0104$, the effective area of the silver stearate surface is 25 times greater than the effective area of the silver halide surface (Goryaev 1994b).

Electronic microscope scanning has indicated that particles of silver stearate are oblong prisms (Fig. 3). The base length of these prisms is 3 to 5 times less than their height. The cube crystals of silver bromide were detected on the prism particles of silver stearate. In this case $\frac{s'}{s} \approx 30$. Thus, the above estimate is quite consistent with the optimal concentration values of sensitizing dyes observed in the experiments in photothermographic compositions that are almost two orders of magnitude greater than the values for traditional photographic emulsions (Goryaev, Kolesova, Timohina et al. 1992).

A luminescence light hits on the surface of the AgBr microcrystal via the lightguide mechanism shown in Fig 4. It is worth noting that the luminescence light of dye molecules hits the silver halide microcrystal both directly and when reflected from the interior face of a silver stearate particle. The reason for this is that silver stearate has a relatively high refractive index of 1.515 (Goryaev, Smirnov 2012). In turn, the refractive index of the environment (with polyvinyl butyral as the binder) is 1.485 (Kabanov 1974).

As a result, the luminescence light in silver stearate attains total internal reflection at angles of incidence of about 75° to 80°. At the interface of silver stearate and silver halide—the refractive index of silver bromide in visible range is over 2.2 (White 1972)—the luminescence light efficiently passes into AgBr. Thus, the silver stearate particle, similarly to a lightguide, focuses the light emitted by the dye localized on the silver stearate surface to a significant degree (Goryaev 1994b). In turn, this luminescence light is effectively absorbed by silver bromide sensitized by dye; the effect of the luminescence light of the dye molecules on silver stearate becomes significant. It is interesting to note that the adsorbed dye Rhodamine
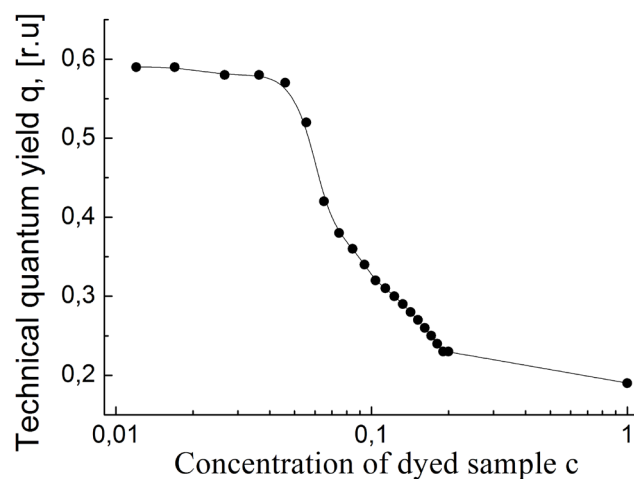
Fig. 1. The dependence of the luminescence technical yield of Rhodamine 6G adsorbed on the surface of silver stearate on the degree of the dilution by "white standard" (magnesium oxide).
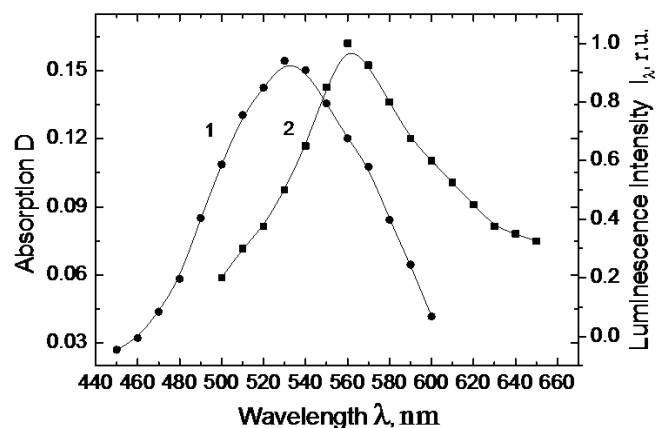
Fig. 2. Absorption (1) and luminescence (2) spectra of Rhodamine 6 G adsorbed on silver stearate surface
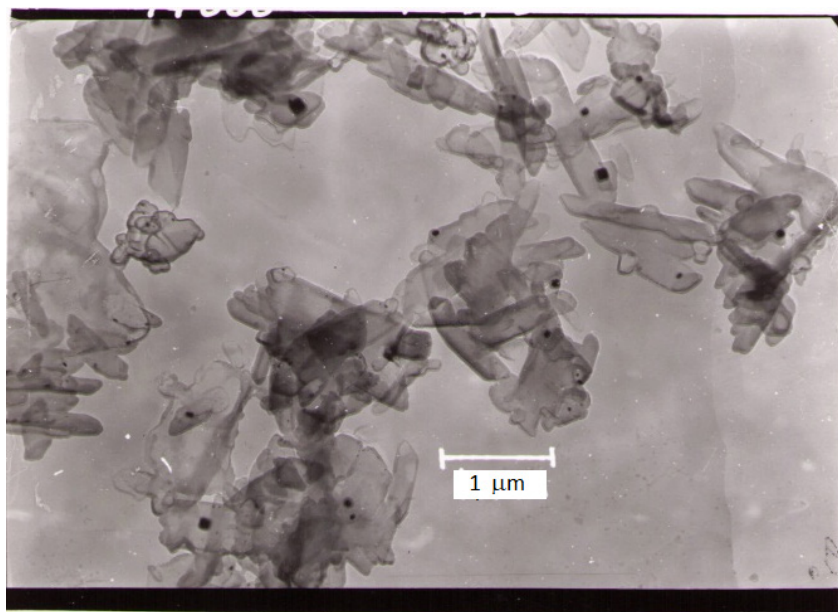
Fig. 3. Electron microphotographs of the silver stearate particles with the AgBr microcrystals located on its surface. The zoom is 14000x
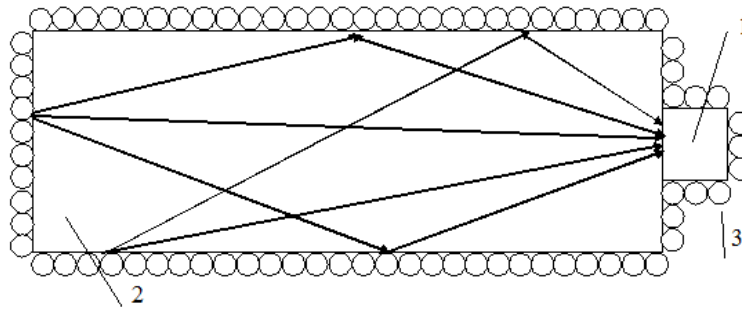
Fig. 4. Lightguide mechanism scheme of spectral sensitization of photothermographic materials. 1 – AgBr, 2 – silver stearate, 3 – adsorbed dye molecules.
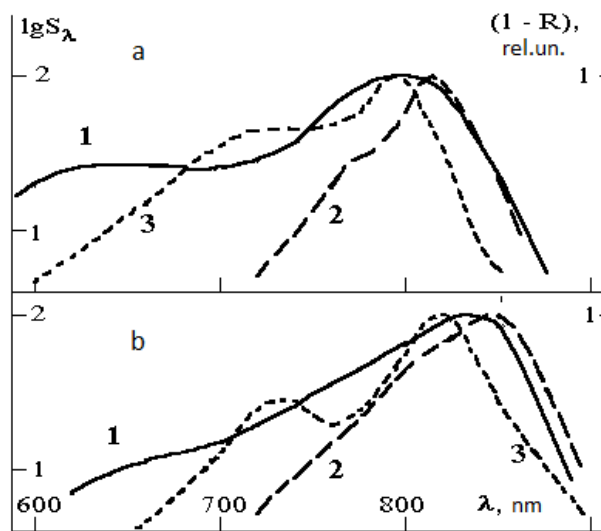
Fig. 5. Dependences of the spectral sensitivity of the photothermographic films based on silver bromide and silver stearate (1) and traditional silver-bromide emulsions (2) sensitized by no. 1389 (a) and no. 722 (b) dyes, the diffuse reflective spectra of these dyes (3)

6G increases the dielectric permittivity of silver stearate (Smirnov, Castro, Goryaev et al. 2017), which leads to an increase in the role of the lightguide sensitization mechanism. In order to estimate the contribution of dyes adsorbed on a non-light-sensitive organic silver salt to the process of spectral sensitization, a study into the spectral sensitivity of photo layers and absorption of dyes was carried out (Goryaev 1998). Figure 5 shows the dependences of the spectral sensitivity of the photothermographic films based on silver bromide and silver stearate (curve 1) and traditional silver-bromide emulsions (curve 2) sensitized by the same infra-chromatic dyes (Goryaev, Shapiro 1997). Also, the diffuse reflectance spectra of these dyes adsorbed on silver stearate are presented (curve 3).

Usually, the spectral dependence of the sensitivity S_λ of photographic materials follows the course of the light absorption by adsorbed dyes, except in cases of simultaneous adsorption of the various aggregate forms of dye. Therefore, the spectral dependence of the sensitivity of the silver-bromide emulsion (curves 2, Fig. 5) corresponds to the absorption spectrum of the dyes adsorbed on AgBr. Figure 5 shows that the position of the absorption bands of the dyes adsorbed on silver bromide and silver stearate differs significantly, and the spectral sensitivity of photothermographic composition is determined by the superposition of their absorption spectra. A qualitative comparison of the spectral dependences shown in fig. 5 allows for the conclusion that the contributions of the dyes adsorbed on silver bromide and the dyes adsorbed on silver stearate in the spectral sensitization process are approximately equal.

References

Akimov, I. A., Cherkasov, U. A., Cherkashin, M. I. (1980) *Sensibilizirovannyj fotoeffekt [Sensitized photoeffect].* Moscow: Nauka Publ., 384 p. (In Russian)

Ermolaev, V. L., Sveshnikova, E. B., Bodunov, E. N. (1996) Inductive-resonant mechanism of nonradiative transitions in ions and molecules in condensed phase. *Physics-Uspehi*, 39 (3), 261–282. DOI: 10.1070/PU1996v039n03ABEH000137 (In English)

Goryaev, M. A. (1980) Metod opredeleniya spektral'no-lyuminestsentnykh kharakteristik poroshkoobraznykh sistem [Method of determining the luminescence spectra of powder system]. *Pis'ma v zhurnal tekhnicheskoj fiziki*, 6 (11), 1132–1135. (In Russian)

Goryaev, M. A. (1981) Kvantovyj vykhod i spektry lyuminestsentsii krasitelej v adsorbirovannom sostoyanii [Quantum yield and luminescence spectra of dyes in adsorbed condition]. *Optika i spektroskopiya*, 51 (6), 1016–1020. (In Russian)

Goryaev, M. A. (1991) Termoproyavlyaemye fotomaterialy na osnove neorganicheskikh sistem [Heat-development photomaterials based on inorganic systems]. *Zhurnal nauchnoj i prikladnoj fotografii*, 36 (5), 421–430. (In Russian)

Goryaev, M. A. (1994a) Upravlenie fotokhimicheskoj chuvstvitel'nost'yu termicheski proyavlyaemykh serebryanykh materialov [Control of photochemical sensitivity of thermally developable silver materials]. *Zhurnal prikladnoj khimii*, 67 (6), 963–966. (In Russian)

Goryaev, M. A. (1994b) Svetovodnyj mekhanizm spektral'noj sensibilizatsii krasitelyami fotoprotsessov v sisteme dielektrik-poluprovodnik [Lightguide mechanism of spectral sensitization of photoprocesses with dyes in an insolator-semiconductor system]. *Pis'ma v zhurnal tekhnicheskoj fiziki*, 20 (21), 40–43. (In Russian)

Goryaev, M. A. (1998) Dopolnitel'nye puti povysheniya effektivnosti spektral'noj sensibilizatsii fototermograficheskikh sistem [Additional ways for enhancing spectral sensitization of photothermographic materials]. *Zhurnal nauchnoj i prikladnoj fotografii*, 43 (3), 1–8. (In Russian)

Goryaev, M. A. (2011) Sensibilizatsiya fotoprotsessov v registriruyushchikh sredakh [Sensitization of the photoprocesses in registration medium]. In: G. A. Bordovskij (ed.). *Fizika neuporyadochennykh i nanostrukturirovannykh oksidov i khal'kogenidov metallov [Physics of disordered and nanostructured metal oxides and chalcogenides].* Saint Petersburg: Herzen State Pedagogical University of Russia Publ., 306–326. (In Russian)

Goryaev, M. A. (2013) *Fizicheskie osnovy fotokhimii tverdogo tela. Fotoliz neorganicheskikh tverdykh tel [Physical basis of photochemistry of a solid. Photolysis of inorganic solids].* Saarbrucken: LAP Lambert Academic Publishing, 144 p. (In Russian)

Goryaev, M. A., Kolesova, T. B., Timohina, M. N., Gulkova, I. M. (1992) Formirovanie fotograficheskikh svojstv termoproyavlyaemykh fotomaterialov na osnove solej serebra [Formation of the photographic properties of the photothermographic materials based on silver salt]. In: Yu. A. Vasilevskij et al. (eds.). *Tekhnologiya i svojstva materialov dlya zapisi informatsii [Technology and materials properties for data recording].* Moscow: NII Khimfotoproekt Publ., 67–77. (In Russian)

Goryaev, M. A., Shapiro, B. I. (1997) Sensibilizatsiya serebryanykh termoproyavlyaemykh fotomaterialov v blizhnej infrakrasnoj oblasti [Sensitization of silver heat-developable materials to the near-IR range]. *Zhurnal nauchnoj i prikladnoj fotografii*, 42 (2), 65–67. (In Russian)

Goryaev, M. A., Smirnov, A. P. (2012) Spektral'naya sensibilizatsiya fototermograficheskikh materialov i opticheskie svojstva stearata serebra [The spectral sensitization of photothermographic materials and the optical properties of silver stearate]. *Izvestia Rossijskogo gosudarstvennogo pedagogicheskogo universiteta im. A. I. Gertsena — Izvestia: Herzen University Journal of Humanities & Sciences*, 144, 29–36. (In Russian).

Goryaev, M. A., Smirnov, A. P. (2015) Lyuminestsentsiya adsorbirovannogo na stearate serebra krasitelya i sensibilizatsiya fototermograficheskikh materialov [Luminescence of dye adsorbed on silver stearate and sensitization of photothermographic materials]. *Izvestia Rossijskogo gosudarstvennogo pedagogicheskogo universiteta im. A. I. Gertsena — Izvestia: Herzen University Journal of Humanities & Sciences*, 173, 50–54. (In Russian)

Kabanov, V. A. (ed.). (1974) *Entsiklopediya polimerov. T. 2: L — Polinoznye volokna [Polymer encyclopedia. Vol. 2: L — Polynosic viscose rayon fiber].* Leningrad: Sovetskaya entsiklopediya Publ., 1032 columns. (In Russian)

Morgan, D. A. (1993) 3M's dry silver technology — an ideal medium for electronic imaging. *The Journal of Photographic Science*, 41 (3), 108–109. DOI: 10.1080/00223638.1993.11738502 (In English)

Sahyun, M. R. V. (1998) Thermally developable photographic materials (TDPM): A review of the state-of-the-art in mechanistic understanding. *Journal of Imaging Science and Technology*, 42 (1), 23–30. (In English)

Smirnov, A. P., Castro, R. A., Goryaev, M. A., Fomicheva, E. E. (2017) Dielectric relaxation and charge transfer in silver stearate with adsorbed dye Rhodamine 6G layers. *Universitetskij nauchnyj zhurnal — Humanities and Science University Journal*, 27, 69–77. (In English)

White, J. J. (1972) *Optical properties of silver bromide. Journal of the Optical Society of America*, 62 (2), 212–218. DOI: 10.1364/JOSA.62.000212 (In English)

UDC 538.9+537.3

Dielectric relaxation in nanocomposites based on thermoplastic polyimide and carbon nanofibres

H. T. Dao[✉1], R. A. Castro Arata[1], A. A. Kononov[1], N. A. Nikonorova[2]

[1] Herzen State Pedagogical University of Russia, 48 Moika River Emb., Saint Petersburg 191186, Russia
[2] Institute of Macromolecular Compounds of Russian Academy of Sciences, 31 Bolshoy Pr.,
Saint Petersburg 199004, Russia

Authors

Hong T. Dao, e-mail: honghip2012@gmail.com

Rene Alejandro Castro Arata, ORCID: 0000-0002-1902-5801

Alexey A. Kononov, ORCID: 0000-0002-5553-3782

Natalia N. Nikonorova, ORCID: 0000-0002-7928-9227

Abstract. The article presents the study of R-SOD 3% nanocomposite's molecular mobility based on thermoplastic PI (R-SOD) with 3% of carbon nanofibres by dielectric method. Dielectric spectrum shows two processes of dipole polarisation relaxation: in the glassy state (local β process) and in the highly elastic state (cooperative α process) related to molecular mobility of phenyl rings with polar ──O── groups in diamine and dianhydride parts of a macromolecule and to segmented motion, respectively.

Keywords: dielectric relaxation, polymeric composites, polyimide.

Introduction

Recently, polymer nanocomposites have been in especially great demand, since they differ from conventional polymer composite materials by their greater impact and wear resistance, which allows their use in the military and aerospace developments. Polypropylene, polystyrene, polyamide and polyimide are used as a matrix, while particles of aluminium and titanium oxides, carbon as well as silicon nanotubes and fibres act as nanofillers. Introducing nano-additives of different nature and concentration makes it possible to change their mechanical, electrical, thermal, optical and other characteristics. Nanocomposite membranes based on thermoplastic polyimides PI (heat treatable), which are actively used as thermostable coatings resistant to water and chemical attack, are of special interest.

The properties of nanocomposites, studied by various methods, depend not only on the chemical structure of the matrix and the nature of nanoparticles, but also on interaction between them. The intramolecular and intermolecular interactions in a nanocomposite can be evaluated by molecular mobility (McCrum, Read, Williams 1967; Hedvig 1977). One of the traditional methods for studying molecular mobility is dielectric spectroscopy (DS). The DS method serves as a tool for discovering specific features of polarisation processes and their relationships with structural features of the studied material.

This work uses the dielectric method to investigate the molecular mobility of thermoplastic PI nanocomposite based on R-SOD (see Fig. 1) with 3% of carbon nanofibres. The objective of this study is to determine molecular mechanisms underlying the observed relaxation processes of the dipole polarisation.
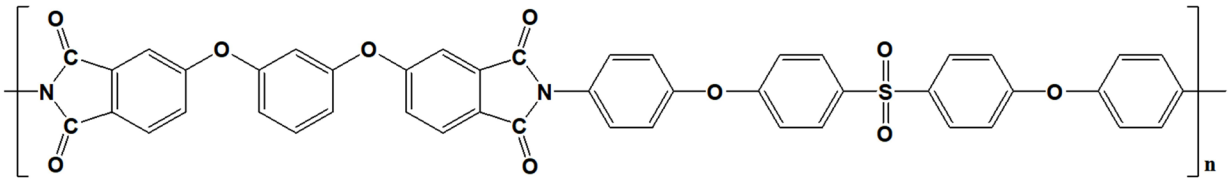
Fig. 1. Structure of R-SOD thermoplastic polyimide

Thermoplastic polyimide (P-SOD) was produced by a two-step synthesis of 1,3-bis(3,4-dicarboxyphenoxy) benzene and 4,4'-bis(4"- aminophenoxy)diphenyl sulfone as well as nanocomposites R-SOD 3% with carbon nanofibres (D × L = 100 nm × 20–200 μm) (Nikonorova, Kononov, Dao, Castro 2019).

The dielectric spectra were obtained with a wideband dielectric spectrometer "Concept 22" and "Concept 81" by Novocontrol Technologies with an automatic high-resolution frequency analyser ALPHA-ANB. Films of 25…40 μm thickness compressed between brass electrodes (the upper electrode diameter of 20 mm) at a temperature of approx. 300 °C above the glass transition temperature (T_g) were taken as samples. The dielectric behaviour was obtained in the 0.1–2E6 Hz frequency range and the 20–3200 °C temperature range.

Dielectric spectra were analysed with the Havriliak-Negami (HN) empirical function (Havriliak, Negami 1967) using the Novocontrol Winfit software. These estimations were used to determine positions of the dielectric loss maxima and the HN parameters for the studied relaxation processes:

$$\varepsilon^*(\omega) = \varepsilon_\infty + \frac{\Delta\varepsilon}{\left[1 + (i\omega\tau)^{\alpha_{HN}}\right]^{\beta_{HN}}} \tag{1}$$

where ε_∞ is the high-frequency limit of the real part of dielectric permittivity, $\Delta\varepsilon$ is the dielectric increment (the difference between the low- and high-frequency limits), $\omega = 2\pi f$, α_{HN} and β_{HN} are shape parameters that describe the symmetric and asymmetric expansion of the relaxation function, respectively. The most probable relaxation time corresponding to the dielectric loss maximum was evaluated by the formula:

$$\tau_{max} = \tau_{HN}\left[\frac{\sin(\frac{\pi(\alpha_{HN})\beta_{HN}}{2(\beta_{HN}+1)})}{\sin(\frac{\pi(\alpha_{HN})}{2(\beta_{HN}+1)})}\right]^{1/(\alpha_{HN})} \tag{2}$$

Results and discussion

Two regions of the maximum on dielectric spectra resulting from the relaxation processes of the dipole polarization were observed (Fig. 2). These regions are indicated in the order of the temperature increase as β (in the glassy state) and α (in the rubbery state). Another $tg\delta_{max}$ region was observed at temperatures above α process, corresponding to the DC conductivity relaxation not displayed in the figure 1.

Fig. 3 and 4 show the dependence of dielectric loss factor in temperature regions on the β and α relaxation processes, respectively, where symbols indicate experimental points.

Fig. 5 shows the values of relaxation times for β and α processes calculated by formula 2 (symbols) and their temperature dependences (lines) calculated according to the formulas 3 and 4, curve 1 and 2, respectively.

Dependence $-\log\tau_{max} = \phi(1/T)$ for β process can be described by the Arrhenius equation:

$$\tau(T)_{max} = \tau_0 \exp\left(\frac{E_a}{RT}\right) \tag{3}$$

Table 1. Parameters of the Arrhenius equation (3) for β process

Sample	$-\log\tau_0$, s	E_a, kcal/mol
R-SOD 3% fibres	19.8	29
Error (±)	0.1	3

Table 2. Parameters of the equation (4) in α process region for R-SOD 3%

Sample	$-\log\tau_0$, s	B, K	T_0, K	T_g, °C
Р-СОД 3%	11.7	1317	441	222
Error (±)	0.3	46	13	8

T_g is determined at $\tau_{max} = 0$
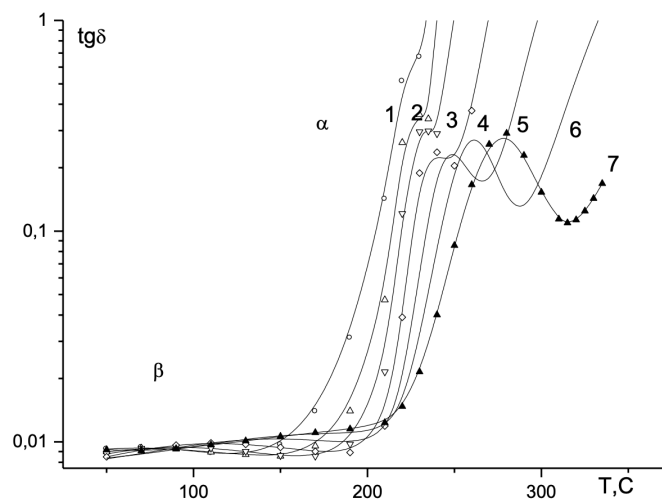
Fig. 2. Temperature dependence of tgδ at 0.1(1), 1(2). 10(3), 100(4), 1000 (5) 10000 (6), and 100000 (7) Hz
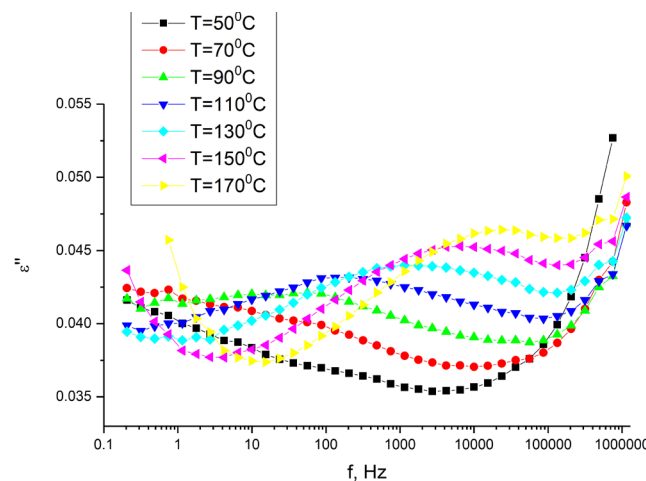
Fig. 3. Frequency dependences of dielectric loss factor process at different temperatures (T see in Figure) for β Symbols are experimental points. Solid lines are approximation by HN formula
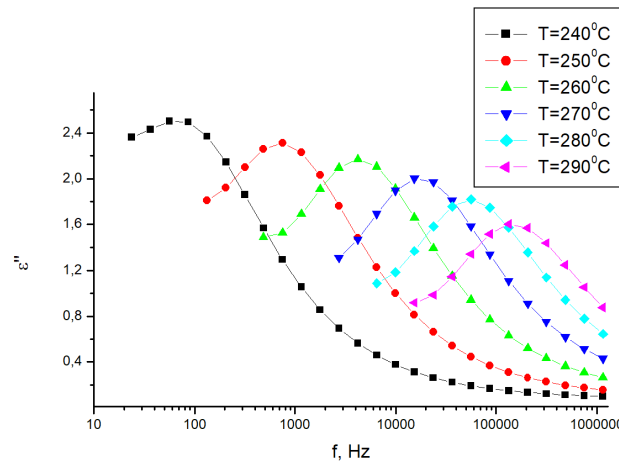
Fig. 4. Frequency dependences of dielectric a loss at different temperatures (T see in Figure) for α process. Symbols are experimental points. Solid lines are approximation by HN formula
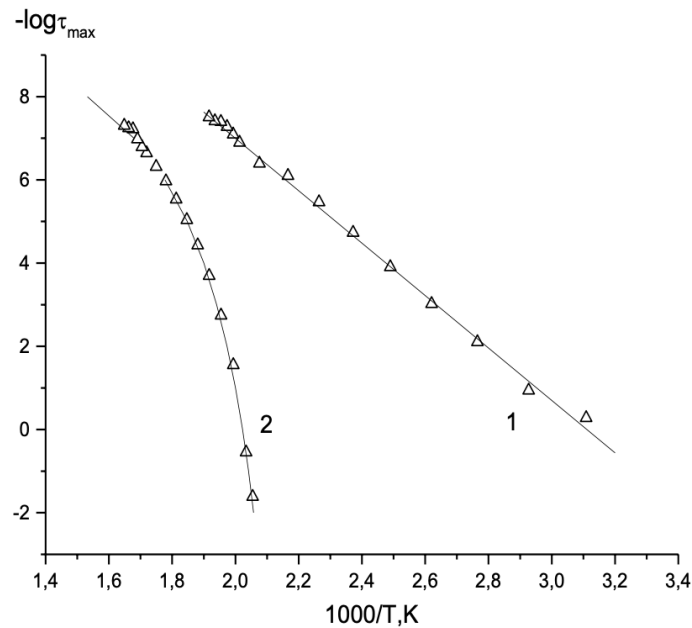
Fig. 5. Temperature dependence of the relaxation time calculated by the HN formula in the region of β (curve 1) and α process (curve 2)

where $\tau_0 = \tau_{max}$ at $T = \infty$, E_a is the activation energy and R is the universal gas constant (R = 8.314 J/mol.K). The linearity of $-\log\tau_{max} = \phi(1/T)$ dependence is typical for local forms of molecular mobility described by the Debye model. This model assumes the absence of intermolecular interactions, and the activation energy does not depend on temperature here. The equation parameters of formula (3) are presented in Table 1.

In the temperature region corresponding to α relaxation process the values of relaxation time and temperature dependence $-\log\tau_{max} = \phi(1/T)$ reveal a nonlinear curve (Fig. 5, curve 2). This nonlinearity is typical for cooperative relaxation processes which are characterised by a wide set of relaxation times and can be considered as a joint correlated movement of a large number of segments belonging to neighbouring macromolecules. The molecular mobility of kinetic segments depends on the state of the immediate environment and is determined largely by intermolecular interactions. The activation energy of this cooperative process depends on the temperature, and $-\log\tau_{max} = \phi(1/T)$ dependences are well described by the empirical Vogel–Tammann–Fulcher (VTF) equation (Kremer, Schöonhals 2012):

$$\tau_{max} = \tau_o \exp(\frac{B}{T - T_0}) \tag{4}$$

where τ_0, B, and T_0 are temperature-independent parameters. T_0 is the so-called Vogel temperature. B parameter is a cooperativity measure of the relaxation process. The smaller B is, the greater distortion and deviation from linearity of $-\log\tau_{max} = \phi(1/T)$ dependence as well as the cooperativity of the process are. Parameters of the equation (4) for α process are given in Table 2.

According to the data obtained earlier for linear thermoplastic PIs of various structures, it can be assumed that appearance of the β process reflects limited rotations of phenyl rings and associated ——O—— polar groups.

Regarding α relaxation for thermoplastic PIs of various structures studied previously, this process can be explicitly associated with the glass transition temperature. The molecular source of α process is the large-scale segmental mobility of the macromolecule ridge (Bryant 2006). The temperature-frequency coordinates of α process (Fig. 5, curve 2), dependence $-\log\tau_{max} = \phi(1/T)$, separate the glassy state region of the polymer (right) from the rubbery state region (left). The glass transition temperature, T_g (see Table 2), was determined by extrapolation of $-\log\tau_{max} = \phi(1/T)$ dependence described by the VTF equation to $-\log\tau_{max} = 0$, ($\tau_{max} = 1$ s). For linear polymers, T_g is determined primarily by intermolecular and dipole-dipole interactions between macromolecules. In the case of PIs, the major contribution to intermolecular interactions is probably provided by dispersion forces between planar phenylene rings.

Conclusion

The molecular mobility of the aromatic thermoplastic polyimide R-SOD with 3% of fibres was studied by the dielectric method. In the studied temperature-frequency range, the dielectric spectra showed two relaxation areas of dipole polarization: α (in the glassy state) and β (in the rubbery state). The empirical formula of HN is used for the quantitative description of relaxation processes.

Comparing dielectric behaviour of polymers having similar structure and the given polyimide allows us to identify relaxation processes. The β process, which is the imposition of several molecular mobility modes with close relaxation times, is associated with the mobility of phenyl rings in the diamine and dianhydride parts of the macromolecule and the polar groups adjacent to them.

The temperature dependence $-\log\tau_{max} = \phi(1/T)$ in α process region displays as a non-linear curve, which is typical for cooperative segmented molecular motion. In the case of the studied system, the major contribution to the intermolecular interactions could be provided by dispersion forces between planar phenylene rings.

This work is devoted to dielectric study of R-SOD 3%. However, in reality, we have in our disposition a series of nanocomposites R-SOD with 1, 3, 4 and 5% nanofibres, as well as pure R-SOD. Preliminary data show that R-SOD 1, 3, and 4% have the dielectric behaviour that differs slightly from pure R-SOD. The dielectric behaviour of R-SOD 5% changes dramatically, indicating the presence of pass-through conductivity (percolation). The next article will present results of a study concerning pure R-SOD and R-SOD 1, 4, and 5%.

References

Bryant, R. G. (2006) Polyimides. In: *Encyclopedia of polymer science and technology.* 4th ed. [Online]. Available at: https://onlinelibrary.wiley.com/doi/pdf/10.1002/0471440264.pst272.pub2. DOI: 10.1002/0471440264.pst272. pub2 (In English)

Havriliak, S., Negami, S. (1967) A complex plane representation of dielectric and mechanical relaxation processes in some polymers. *Polymer*, 8, 161–210. DOI: 10.1016/0032-3861(67)90021-3 (In English)

Hedvig, P. (1977) *Dielectric spectroscopy of polymers.* Bristol: Adam Hilger Ltd., 430 p. (In English)

Kremer, F., Schönhals, A. (eds.). (2012) *Broadband dielectric spectroscopy*, Berlin; Heidelberg: Springer, 729 p. DOI: 10.1007/978-3-642-56120-7 (In English)

McCrum, N. G., Read, B. E., Williams, G. (1967) *Anelastic and dielectric effects in polymeric solids.* London; New York: John Wiley, 617 p. (In English)

Nikonorova, N. A., Kononov, A. A., Dao, H. T., Castro, R. A. (2019) Molecular mobility of thermoplastic aromatic polyimides studied by dielectric spectroscopy. *Journal of Non-Crystalline Solids*, 511, 109–114. DOI: 10.1016/j. jnoncrysol.2018.12.032 (In English)

Some remarks on the naked singularity phenomenon

V. D. Vertogradov[⊠1]

[1] Herzen State Pedagogical University of Russia, 48 Moika River Emb., Saint Petersburg 191186, Russia

Author
Vitalii D. Vertogradov,　e-mail: vdvertogradov@gmail.com

Abstract. This paper describes a naked singularity phenomenon. The study presents necessary definitions
and methods for dealing with this effect. Moreover, the article gives two explicit examples of the naked
singularity formation.

Keywords: gravitational collapse, naked singularity, strength of singularity, black hole, Vaidya spacetime.

Introduction

Black holes are among the most appealing fields of modern theoretical physics. In 1916 Schwarzschild solved the Einstein equation and showed that there is a line at where all physical quantities are blown up. This is called a singularity. All famous black hole models have a singularity which is hidden under the event horizon. In 1970, Penrose came up with the cosmic censorship principle (CCP). According to this principle, all singularities must be hidden under the event horizon. However, all these models describe eternal black holes without mentioning anything about their formation. Therefore, in order to understand how a black hole is formed, it is necessary to consider gravitational collapse.

In 1939, Oppenheimer and Snyder (Oppenheimer, Snyder 1939) considered gravitational collapse of the pressureless homogeneous matter cloud. They showed that such a collapse results in a black hole. A black hole was believed to be the only result of gravitational collapse for a long time. However, later it was found that a singularity might be formed earlier than the apparent horizon during gravitational collapse (see Joshi 2007; Goswami, Joshi 2007). An apparent horizon is a marginally trapped surface and a boundary of the trapped region. Thus, if it is absent and there is a family of non-spacelike future-directed geodesics which terminate at the central singularity in the past, then such a singularity is visible and is called a naked singularity. If we consider gravitational collapse of the unhomogeneous dust, then the result of such a collapse might be a naked singularity. It should be noted that naked singularity is temporary, and in a short period of time it is covered with the apparent horizon, which results in a black hole.

Naked singularity formation violates CCP in its original version. However, after 1970 other CCPs were formulated and one of them admits naked singularity formation in four-dimensional spacetime (for details on all CCPs, see Joshi 2007).

When gravitational collapse is considered, vacuum solutions cannot be considered anymore. We must put the energy-momentum tensor (EMT) on the right side of the Einstein equation. The EMT must be physically relevant and must satisfy energy conditions: weak, strong and dominant ones (Hawking, Ellis 1973). Nowadays there are a lot of gravitational collapse models which result in naked singularities (Goswami, Joshi 2007; Vertogradov 2016; 2018; Mkenyeley, Goswami, Maharaj 2014); however, if the EMT satisfies all necessary energy conditions, these naked singularities are temporary. Nevertheless, one en-

ergy condition—the strong one—can be violated. In this case matter distribution is thought to possess negative pressure and an eternal naked singularity might be formed (Goswami, Joshi 2007; Vertogradov 2018). It should be noted that in this case 'eternal' means that the singularity is formed during the gravitational collapse process and will never be covered with the apparent horizon.

This paper has the following structure. Section II provides definitions of all necessary terms such as 'energy condition', 'apparent horizon', 'expansion', etc. Section III describes naked singularity formation in the general spherical symmetry case. Section IV gives necessary conditions for the naked singularity formation in case of generalised Vaidya spacetime. Section V presents the violation of the strong energy condition and considers the possibility of eternal naked singularity formation. Section VI is the conclusion. Units $g = c = 1$ are used throughout this paper. Moreover, the "$- + + +$" signature is used in this paper.

$$M' = \frac{\delta M}{\delta r} \, , \dot{M} = \frac{\delta M}{\delta t} = \frac{\delta M}{\delta v}$$

are partial derivatives with respect to coordinate r and time t and v, respectively.

Necessary definitions

The energy condition

When gravitational collapse is considered, the EMT is put on the right side of Einstein equations. However, the EMT must obey certain conditions since these models should be physically relevant and should never have negative mass or negative energy density, etc. Therefore, it is possible to impose conditions that energy density must be positive, or that energy density must be more than pressure (Hawking, Ellis 1973; Poisson 2004).

The following energy conditions are imposed: the weak, strong and dominant energy conditions.

Weak energy condition.
Energy density of any matter distribution measured by an observer at any spacetime point must be positive or equal to zero.

Let v^i be four-velocity of an observer; then the weak energy condition can be written as

$$T_{ik}v^i v^k \geq 0 \, , \tag{1}$$

where T_{ik} is the energy-momentum tensor.

The strong energy condition demands that

$$R_{ik}v^i v^k \geq 0 \, , \tag{2}$$

where R_{ik} is the Ricci tensor.

If matter distribution is a perfect fluid, then the condition (2) gives

$$\rho + P \geq 0 \, . \tag{3}$$

where ρ and P are energy density and pressure, respectively.

Dominant energy condition.
Any matter distribution must move along non-spacelike worldlines. For any non-spacelike vector v^i this condition gives

$$-T_k^i v^k = tlnvf \, , \tag{4}$$

where $tlnvf$ stands for the timelike or null vector field. It means that this vector must be a non-spacelike one. The condition (4) gives

$$\rho \geq P \, . \tag{5}$$

For most known matter distributions, all three conditions are valid. However, there are some models where one of the conditions is violated. For example, the strong energy condition is violated inside a regular black hole (Dymnikova 1992; 2002).

The strength of the central singularity

We must understand that singularities which we consider must be genuine and cannot be removed by proper coordinate transformation. If a singularity can be removed, then it is weak; if it cannot be removed, then it is a strong one. A singularity is called gravitationally strong or simply strong if it destroys any object that falls into it by stretching or crushing. If not, such a singularity is called gravitationally weak (Nolan 1999).

According to the Tipler's definition (Tipler 1977), a singularity is gravitationally strong if

$$\lim_{\tau \to 0} \tau^2 R_{ik} k^i k^k \geq 0 \,, \tag{6}$$

where τ is an affine parameter and k^i is a tangent vector to a non-spacelike geodesic.

The apparent horizon

An apparent horizon is a marginally trapped surface (Faraoni 2015) and a border of the trapped region. To calculate the apparent horizon (Poisson 2007), it is necessary to take the geodesic congruence and the vector u^i which is tangent to this congruence

$$u^i_{;k} u^k = \alpha u^i \,, \tag{7}$$

where ';' is a covariant derivative, and α shows the failure of u^i to be parallel transported along the congruence. If $\alpha = 0$, the u^i vector is parallel transported along the geodesic.

First of all, the expansion θ should be defined. There are two cases:

$$\theta = u^i_{;i} \,, \tag{8}$$

if $\alpha = 0$, and

$$\theta = e^\gamma (u^i_{;i} - \alpha) \,, \tag{9}$$

if $\alpha \neq 0$. Here is a coefficient which does not have any impact on the apparent horizon definition. A surface is called a trapped one if $\theta < 0$ everywhere on this surface. The apparent horizon, as said earlier, is a border of the trapped region and can be defined as

$$\theta = 0 \,. \tag{10}$$

It follows from (10) that the parameter (9) does not have any impact on the apparent horizon definition.

The general case

The most general spherically symmetric metric in comoving coordinates $\{t, \kappa, \theta, \varphi\}$ has the following form (Joshi 2007):

$$ds^2 = -e^{2\mu} dt^2 + e^{2\psi} dr^2 + R^2 d\Omega^2 \,, \tag{11}$$
$$d\Omega^2 = d\theta^2 + \sin^2\theta d\varphi^2 \,.$$

Here

$$\mu = \mu(r,t) \,,$$
$$\psi = \psi(r,t) \,, \tag{12}$$
$$R = R(r,t) \,.$$

The EMT in the case of a perfect fluid is determined by

$$T_{ik} = (\rho + P)u_i u_k + P g_{ik} \,, \tag{13}$$

where P and ρ are pressure and density, respectively, and u_i is four-velocity.

In any comoving frame the EMT for the first type of the matter field (i.e. for any physically relevant matter such as dust, perfect fluid, scalar fields, etc.) has the form

$$
\begin{aligned}
T^{00} &= -\rho(r,t)\,, \\
T^{11} &= P_r(r,t)\,, \\
T^{22} &= T^{33} = P_\theta(r,t),
\end{aligned}
\tag{14}
$$

where P_r and P_θ are radial and tangent pressure components, respectively.

If there is a family of non-spacelike future-directed geodesics which terminate at the central singularity in the past, and if the time of the singularity formation is less than the time of the apparent horizon formation, then the result of the collapse is a naked singularity. According to Joshi (2007), the result of such a collapse depends on the initial profile data.

The equation of the apparent horizon in case of a general spherically symmetric metric (11) is

$$g^{ik} R_{,i} R_{,k} = 0 \,. \tag{15}$$

A radial null geodesic is defined as

$$\frac{dt}{dr} = e^{2(\psi-\mu)} \,. \tag{16}$$

If the equation (15) cannot be satisfied, then the apparent horizon is absent. And if the condition

$$x_0 = \lim_{t\to 0\,,\, r\to 0} \frac{dt}{dr} \geq 0 \tag{17}$$

is satisfied and the value x_0 is finite, then the singularity at $r = 0$ and at the time $t = 0$ is a naked one.

In this case there is a family of non-spacelike future directed geodesics which terminate at the central singularity in the past. It means that an external observer can observe processes near this region with extremely high energy density.

The temporary naked singularity in generalised Vaidya spacetime

This paper considers gravitational collapse of thin radiating shells (Vertogradov 2016). The first shell collapses at the central singularity at $r = v = 0$ where $M(0,0) = 0$. During the collapse of other shells the mass function is growing, and when the last shell collapses, the mass function becomes a well-known Schwarzschild mass. This article only considers shell-focusing singularities, while shell-crossing singularities are gravitationally weak and irrelevant to this study. If there is a family of non-spacelike future-directed geodesics which originate at the central singularity in the past, and if the time of the singularity formation is less than the time of the apparent horizon formation, then the result of such a gravitational collapse is a naked singularity. If there is no such family of geodesics, or the time of the apparent horizon formation is less than the time of the singularity formation, then the result is a black hole.

Generalised Vaidya spacetime corresponds to the combination of two matter fields of types I and II (where type I is the usual matter and type II goes along null geodesics) which is generally described by the equation (Wang, Yu 1999)

$$
\begin{aligned}
ds^2 &= -e^{2\psi(v,r)}\left(1 - \frac{2M(v,r)}{r}\right)dv^2 + 2\varepsilon e^{\psi(v,r)}dvdr + r^2 d\omega^2 \,, \\
d\omega^2 &= d\theta^2 + \sin^2(\theta)d\varphi^2 \,,
\end{aligned}
\tag{18}
$$

where $M(v,r)$ is the mass function depending on coordinates r and v which correspond to advanced/retarded time, means $\varepsilon = \pm 1$ ingoing/outgoing radiating thin shells, respectively.

If we consider gravitational collapse, then $\varepsilon = +1$. With a suitable choice of coordinates, it is possible to set $\psi(v,r) = 0$. So, equation (18) now can be written as

$$ds^2 = -\left(1 - \frac{2M(v,r)}{r}\right)dv^2 + 2\varepsilon dvdr + r^2 d\omega^2 . \tag{19}$$

The energy momentum tensor can be written as

$$T_{ik} = T_{ik}^{(n)} + T_{ik}^{(m)} , \tag{20}$$

where the first term corresponds to the matter field of type I, and the other one corresponds to the matter field type II.

The expression of the energy momentum tensor can be expressed as follows:

$$
\begin{aligned}
T_{ik}^{(n)} &= \mu L_i L_k , \\
T_{ik}^{(m)} &= (\rho + P)(L_i N_k + L_k N_i) + P g_{ik} , \\
\mu &= \frac{2\dot{M}}{r^2} , \\
\rho &= \frac{2M'}{r^2} , \\
P &= -\frac{M''}{r} , \\
L_i &= \delta_i^0 , \\
N_i &= \frac{1}{2}\left(1 - \frac{2M}{r}\right)\delta_i^0 - \delta_i^1 , \\
L_i L^i &= N_i N^i = 0 , \\
L_i N^i &= -1 ,
\end{aligned}
\tag{21}
$$

where P means pressure, ρ means density and L, N mean two null vectors (Wang, Yu 1999).

Strong and weak energy conditions demand the followng:

$$
\begin{aligned}
\mu &\geq 0 , \\
\rho &\geq 0 , \\
P &\geq 0 .
\end{aligned}
\tag{22}
$$

The dominant energy condition imposes the following conditions on the energy momentum tensor:

$$
\begin{aligned}
\mu &\geq 0 , \\
\rho &\geq P \geq 0 .
\end{aligned}
\tag{23}
$$

Let us consider the simplest case, when the equation of the state is

$$P = \frac{\rho}{3} . \tag{24}$$

(The results for the equation of the state $P = \beta\rho$ where β belongs to the interval $(0, \frac{1}{3})$ are the same (Vertogradov 2016).

If the equation (21) is applied, the mass function is obtained:

$$3M''(v,r)r + 2M'(v,r) = 0 , \tag{25}$$

$$M(v,r) = C(v) + D(v)r^{\frac{1}{3}} .$$

Pressure and density are defined as

$$\rho = \frac{2}{3}\frac{D(v)}{r^{\frac{8}{3}}} \, ,$$

$$P = \frac{2}{9}\frac{D(v)}{r^{\frac{8}{3}}} \, . \tag{26}$$

Strong, weak and dominant energy conditions demand that

$$D(v) \geq 0 \, ,$$

$$\dot{C}(v) + \dot{D}(v)r^{\frac{1}{3}} \geq 0 \, , \tag{27}$$

$$C(v) \geq 0 \, .$$

Moreover, the condition $M(0,0) = 0$ demands that

$$C(0) = 0 \, . \tag{28}$$

The equation of the apparent horizon is

$$r = 2C(v) + 2D(v)r^{\frac{1}{3}} \, . \tag{29}$$

Thus, when is the time of the singularity formation, the equation of the apparent horizon is

$$r = 2D(0)r^{\frac{1}{3}} \, . \tag{30}$$

If $D(0) > 0$, then $r > 0$ and the time of the apparent horizon formation is less than the time of the singularity formation; in this case, a black hole is a result of gravitational collapse. Thus, naked singularity is only formed when $D(0) = 0$.

Let us consider if there exists a family of non-spacelike future-directed geodesics which originate at the central singularity $r = v = 0$ in the past. Firstly, it is necessary to substitute the mass function (25) into the geodesic equation

$$\frac{dv}{dr} = \frac{2r}{r - 2(C(v) + D(v)r^{\frac{1}{3}})} \, . \tag{31}$$

If the limit is considered at $r \to 0$, $v \to 0$ in (31), then conditions for the mass function, necessary for the gravitational collapse to result in a naked singularity, are as follows:

$$D(0) = 0 \, ,$$

$$\lim_{v \to 0, r \to 0} \frac{C(v)}{r} = a \geq 0 \, ,$$

$$\lim_{v \to 0, r \to 0} \frac{D(v)}{r^{\frac{2}{3}}} = b \geq 0 \, , \tag{32}$$

$$2a + 2b < 1 \, ,$$

where a, b are arbitrary constants.

Thus, when the conditions (32) are satisfied, the collapse results in a naked singularity. Let us consider an explicit example.

Let

$$C(v) = \alpha v \, , \alpha \geq 0 \, ,$$

$$D(v) = \beta v \, , \beta \geq 0 \, . \tag{33}$$

The condition $D(0) = 0$ is satisfied; therefore, it is necessary to consider whether a family of non-spacelike future-directed geodesics exists. For this purpose, (33) is substituted into (31):

$$\frac{dv}{dr} = \frac{2r}{r - 2\alpha v - 2\beta v r^{\frac{1}{3}}} \, . \tag{34}$$

Now let us use the definition $x_0 = \lim\limits_{r \to 0, v \to 0} \frac{dv}{dr}$ in (34):

$$x_0 = \frac{2}{1 - 2\alpha x_0} \, , \tag{35}$$
$$2\alpha x_0^2 - x_0 + 2 = 0 \, .$$

It should be noted that for a family of non-spacelike future-directed geodesics to exist, it is necessary and sufficient that one root of the equation (35) should be positive. It is possible if

$$\alpha < \frac{1}{8} \, . \tag{36}$$

If the condition (36) is satisfied, then the singularity is naked.

The negative pressure case in generalised Vaidya spacetime

In this case the equation of the state $P = -\frac{1}{2}\rho$ is considered. Then the mass function is given by

$$M(v, r) = c(v) + d(v)r^2 \, . \tag{37}$$

In this model the strong energy condition is violated, because $P < 0$. Weak and dominant energy conditions demand that

$$\dot{c}(v) + \dot{d}(v)r^2 \geq 0 \, , \, d(v) \geq 0 \, . \tag{38}$$

Since $M(0, 0) = 0$, it follows that $c(0) = 0$.
Substituting this solution into the equation of the apparent horizon, we find

$$1 - \frac{2M(v, r)}{r} = 0 \, , \tag{39}$$
$$1 - 2d(v)r - \frac{2c(v)}{r} = 0 \, .$$

When $c(0) = 0$ and $d(0) = 0$, the apparent horizon is absent. Solving this equation with respect to r gives

$$2d(v)r^2 - r + 2c(v) = 0 \, , \tag{40}$$
$$D = 1 - 16c(v)d(v) \, .$$

It follows that the apparent horizon is absent when $(v)d(v) > \frac{1}{16}$. Thus, the naked singularity formation is present when $v = 0$, when the apparent horizon appears, and later when $c(v)d(v) > \frac{1}{16}$; then the apparent horizon disappears again.

The next question under consideration is the existence of non-spacelike future-directed geodesics which terminate at the singularity in the past. For example, let us consider the radial null geodesics equation

$$\frac{dv}{dr} = \frac{2r}{r - 2c(v) - 2d(v)r^2} \, . \tag{41}$$

Let us denote $\lim\limits_{r \to 0, v \to 0} \frac{dv}{dr} = x_0$, then we can substitute $d(v) = \xi v$ and $c(v) = \lambda v$ (where λ, ξ are real

positive constants) in the geodesics equation and rewrite it as

$$x_0 = \frac{2}{1 - 2\lambda x_0} \, ,$$
$$2\lambda x_0^2 - x_0 + 2 = 0 \, , \tag{42}$$
$$x_{0\pm} = \frac{1 \pm \sqrt{1 - 16\lambda}}{4} \, .$$

The family of non-spacelike future-directed geodesics exists if there exists a positive root for the equation above. x_{0+} is positive, but λ should be limited as

$$1 - 16\lambda \geq 0 \to \lambda \leq \frac{1}{16} \, . \tag{43}$$

The result of such a collapse might be a naked singularity.

At the late stage of v, expression (40) has two positive roots. Thus, there are three regions:

- region I, where $\theta < 0 \to 0 \leq r < r_1$,
- region II, where $\theta > 0 \to r_1 < r < r_2$,
- region III, where $\theta < 0 \to r_2 < r < +\infty$.

Let us consider the expansion θ:

$$\theta = e^{-\gamma} \frac{2}{r} \left(1 - \frac{2c(v) + 2d(v)r^2}{r} \right) \tag{44}$$

where e^{γ} has no impact on the sign of θ.

As it follows from (44):

$$\theta < 0 \to 0 \leq r < r_1 \, ,$$
$$\theta > 0 \to r_1 < r < r_2 \, , \tag{45}$$
$$\theta < 0 \to r_2 < r < +\infty \, .$$

This result is similar to Schwarzschild-de Sitter-Kottler spacetime (Faraoni 2015), but with the equation of the state $P = -\frac{1}{2}\rho$. It is clear that region I is a black hole solution with a singularity in its center. If an observer is located in region II, then he can not get information from regions I and III.

In this case the result of the gravitational collapse might be a naked singularity; however, it is temporary and in a very short period of time it is covered with the apparent horizon. However, this is a white hole apparent horizon, because it follows from (44) that $\theta > 0$ at $0 < r < r_2$. In this case, $r_1 < 0$. Thus, there is a region of spacetime where geodesics cannot get into region $0 < r < r_2$ from region $r_2 < r < +\infty$. This white hole is shrinking. At the late stage of v the expression (44) has two positive roots. Then two apparent horizons merge, and the collapse results in a singularity, which is similar to the singularity of the future in Friedman model.

A naked singularity is eternal if there is a family of non-spacelike future-directed geodesics which terminate at the central singularity in the past, the apparent horizon never appears and θ is positive everywhere.

Let us consider the case of the negative pressure when θ is always positive. The equation of the state in this case is $P = -\alpha\rho$, where $1 \leq \alpha < 0$. cannot be more than one due to energy conditions which demand $\rho \geq P \geq 0$. The mass function in this case is defined as

$$M(v, r) = c(v) + d(v)r^{1+2\alpha} \, . \tag{46}$$

The expansion in this case is given by

$$\theta = e^{-\gamma}\frac{2}{r}\left(1 - \frac{2c(v) + 2d(v)r^{1+2\alpha}}{r}\right). \tag{47}$$

Here $e^{-\gamma}$ has no impact on the sign of θ.
Then θ is restricted to positive numbers:

$$\theta > 0 \rightarrow r > 2c(v) + 2d(v)r^{1+2\alpha} . \tag{48}$$

It follows from (48) that this condition can only be satisfied if $c(v) \equiv 0$. Now α is restrictid to $\alpha < 1$, because if $\alpha = 1$, then there is no singularity. The final equation is

$$\theta > 0 \rightarrow 1 - 2d(v)r^{2\alpha} > 0 ,$$
$$r^{2\alpha}d(v) < \frac{1}{2} . \tag{49}$$

It also follows from (49) that there is no apparent horizon, because the condition to the apparent horizon formation is $\theta = 0$, but θ is restricted to $\theta > 0$. Moreover, (49) shows that $d(v)$ must be very small and, therefore, the pressure must be very small, too, because

$$P = -4\alpha(1 + 2\alpha)\frac{d(v)}{r^{2-2\alpha}}$$

In order to prove that there is a family of non-spacelike future-directed geodesics which terminate at the central singularity in the past, it is necessary to consider a null radial geodesic which is given by

$$\frac{dv}{dr} = \frac{2}{1 - 2d(v)r^{2\alpha}} . \tag{50}$$

This family exists if

$$\lim_{v\to 0, r\to 0}\frac{dv}{dr} \geq 0 . \tag{51}$$

However, $\frac{dv}{dr}$ is always positive, because $1 - 2d(v)r^{2\alpha}$ must be positive due to the condition $\theta > 0$.

Thus, all three conditions are satisfied and, according to them, the result of such a collapse is an eternal naked singularity.

Let us look at the equation (49). It has a solution

$$r_{aah} = \left(\frac{1}{2d(v)}\right)^{\frac{1}{1+2\alpha}} . \tag{52}$$

This solution must be matched to the exterior Schwarzschild one. Let r_m be a boundary of two spacetimes. Then there are two cases:

1. $r_{aah} < r_m$,
2. $r_{aah} > r_m$.

In the first case the result of the gravitational collapse is a white hole, because θ is positive at $0 \leq r < r_{ah}$, and there is a family of non-spacelike future-directed geodesics which terminate at the central singularity in the past. However, $\frac{dv}{dr}$ is always positive inside the white hole apparent horizon, and there is no geodesic which can get into the white hole from the region outside of the apparent horizon. But in this case it takes endless time to get to the exterior observer from the singularity.

In case II solutions are matched at r_m, which is less than r_{ah}, and it takes a finite time to get to the exterior observer from the central singularity. Now let us look at the expression of pressure which is given by

$$P = -2\alpha(1 + 2\alpha)\frac{d(v)}{r^{1+2\alpha}}. \tag{53}$$

It follows from equations (49) and (53) that the less the pressure is, the more r_{ah} is. It means that an eternal naked singularity can be formed if the pressure is small enough.

This paper does not consider the question about the strength of the central singularity, but all considered singularities are gravitationally strong (see, for example, Vertogradov 2016; 2018).

Conclusion

This paper briefly explained the naked singularity phenomenon. It identified conditions when a naked singularity might be formed in the case of the most general spherically symmetric metric. Moreover, it presented two explicit examples of the naked singularity formation. This paper considered only spherically symmetric objects. There has been no analytical model for the gravitational collapse of a rotating object proposed so far.

References

Dymnikova, I. (2002) The cosmological term as a source of mass. *Classical and Quantum Gravity*, 19 (4), 725–739. DOI: 10.1088/0264-9381/19/4/306 (In English)

Dymnikova, I. (1992) Vacuum nonsingular black hole. *General relativity and gravitation*, 24 (3), 235–242. DOI: 10.1007/BF00760226 (In English)

Faraoni, V. (2015) *Cosmological and black hole apparent horizons.* Cham: Springer, 199 p. DOI: 10.1007/978-3-319-19240-6 (In English)

Goswami, R., Joshi, P. S. (2007) Gravitational collapse of a self-interacting scalar field. *Modern Physics Letters A*, 22 (01), 65–74. DOI: 10.1142/S0217732307020701 (In English)

Hawking, S. W., Ellis, G. F. R. (1973) *The large scale structure of space-time*. Cambridge: Cambridge University Press, 391 p. DOI: 10.1017/CBO9780511524646 (In English)

Joshi, P. S. (2007) *Gravitational collapse and spacetime singularities.* Cambridge: Cambridge University Press, 273 p. DOI: 10.1017/CBO9780511536274 (In English)

Mkenyeleye, M. D., Goswami, R., Maharaj, S. D. (2014) Gravitational collapse of generalized Vaidya spacetime. *Physical Review D*, 90 (6), 064034. DOI: 10.1103/PhysRevD.90.064034 (In English)

Nolan, B. C. (1999) Strengths of singularities in spherical symmetry. *Physical Review D*, 60 (2), 024014. DOI: 10.1103/PhysRevD.60.024014 (In English)

Oppenheimer, J. R., Snyder, H. (1939) On continued gravitational contraction. *Physical Review*, 56 (5), 455–459. DOI: 10.1103/PhysRev.56.455 (In English)

Poisson, E. (2004) *A relativist's toolkit: The mathematics of black-hole mechanics.* Cambridge, UK; New York: Cambridge University Press, 233 p. DOI: 10.1017/CBO9780511606601 (In English)

Tipler, F. J. (1977) Singularities in conformally flat spacetimes. *Physics Letters A*, 64 (1), 8–10. DOI: 10.1016/0375-9601(77)90508-4 (In English)

Vertogradov, V. D. (2016) Naked singularity formation in generalized Vaidya space-time. *Gravitation and Cosmology*, 22 (2), 220–223. DOI: 10.1134/S020228931602016X (In English)

Vertogradov, V. (2018) The eternal naked singularity formation in the case of gravitational collapse of generalized Vaidya space-time. *International Journal of Modern Physics A*, 33 (17), 1850102. DOI: 10.1142/S0217751X18501026 (In English)

Wang, A., Wu, Y. (1999) Generalized vaidya solutions. *General Relativity and Gravitation*, 31 (1), 107–114. DOI: 10.1023/A:1018819521971 (In English)

In- and out-states of scalar particles confined between two capacitor plates

A. I. Breev[1], S. P. Gavrilov[✉1, 2], D. M. Gitman[1, 3, 4]

[1] Tomsk State University, 36 Lenin Ave., Tomsk 634050, Russia
[2] Herzen State Pedagogical University of Russia, 48 Moika River Emb., Saint Petersburg 191186, Russia
[3] P. N. Lebedev Physical Institute, 53 Leninsky Prospekt, Moscow 119991, Russia
[4] University of São Paulo, 4 Travessa, São Paulo 05508-090, Brazil

Authors

Alexander I. Breev, ORCID: 0000-0001-6038-1288, e-mail: breev@mail.tsu.ru

Sergey P. Gavrilov, ORCID: 0000-0002-0350-3012

Dmitry M. Gitman

Abstract. In this article, a non-commutative integration method of linear differential equations is used to consider the Klein-Gordon-Fock equation with the L-constant electric field with large L, and light cone variables are used to find new complete sets of its exact solutions. These solutions can be related by integral transformations to previously known solutions described by Gavrilov and Gitman (2016b). Then, using the general theory developed by Gavrilov and Gitman (2016a), this article constructs (in terms of new solutions) the so-called in- and out-states of scalar particles confined between two capacitor plates.

Keywords: exact solutions, Klein-Gordon-Fock equation, potential step, strong electric field, non-commutative integration method.

Introduction

Particle production from vacuum by strong electric-like external fields—the Schwinger effect (Schwinger 1951) or the effect of the vacuum instability—is one of the most interesting effects in quantum field theory (QFT) that scientists have already been researching for a long time. The effect can be observable if the external fields are sufficiently strong, e.g. the magnitude of an electric field should be comparable with the Schwinger critical field with $E_c = m^2 c^3 / e\hbar \simeq 10^{16}$ V/cm. Nevertheless, recent progress in laser physics brings hope that an experimental observation of the effect can become possible in the near future (for the review, see Dunne 2009; 2014; Di Piazza, Müller, Hatsagortsyan et al. 2012; Mourou, Tajima 2014; Hegelich, Mourou, Rafelski 2014). Moreover, electron-hole pair creation from vacuum also becomes observable in laboratory conditions in graphene and similar nanostructures (see, e.g. Sarma, Adam, Hwang et al. 2011; Vafek, Vishwanath 2014). Various approaches have been proposed for calculating the effect depending on the structure of such external backgrounds (for a list of relevant publications see Ruffini, Vereshchagin, Xue 2010; Gelis, Tanji 2016). Calculating quantum effects in strong external backgrounds must be non-perturbative with respect to the interaction with strong backgrounds. A general formulation of QED with time-dependent external fields (the so-called *t*-potential steps) was developed by Gitman (1977), Fradkin, Gitman (1981), and Fradkin, Gitman, Shvartsman (1991). It can be also seen that in some situations the vacuum instability effects in graphene and similar

nanostructures caused by strong (with respect of massless fermions) electric fields are of significant interest (see Gelis, Tanji 2016; Allor, Cohen, McGady 2008; Gavrilov, Gitman, Yokomizo 2012; Vafek, Vishwanath 2014; Kané, Lazzeri, Mauri 2015; Oladyshkin, Bodrov, Sergeev et al. 2017; Akal, Egger, Müller et al. 2019 and references therein). At the same time, in these cases electric fields can be considered as time-independent weakly inhomogeneous x-electric potential steps (electric fields of constant direction that are concentrated in restricted space areas) that can be approximated by a linear potential. Approaches for treating quantum effects in the explicitly time-dependent external fields are not directly applicable to the x-electric potential steps. A consistent non-perturbative formulation of QED with critical x-electric potential steps, strong enough to violate the vacuum stability, was constructed in the recent work (Gavrilov, Gitman 2016a). A non-perturbative calculation technique for different quantum processes, such as scattering, reflection, and electron-positron pair creation, was developed there. This technique essentially uses special sets of exact solutions of the Dirac and Klein-Gordon equation with the corresponding external field of x-electric potential steps. The cases when such solutions can be found explicitly (analytically) are called exactly solvable cases. This technique was effectively used to describe particle creation effect in the Sauter field of the form $E(x) = E\cosh^{-2}(x/L_S)$, in a constant electric field between two capacitor plates separated by a distance L (the so-called L-constant electric field), and in exponential time-independent electric steps, where the corresponding exact solutions were available (see Gavrilov, Gitman 2016a; 2016b; Gavrilov, Gitman, Shishmarev 2017). These exactly solvable models make it possible to develop a new approximate calculation method to non-perturbatively treat the vacuum instability in arbitrary weakly-inhomogeneous x-electric potential steps (Gavrilov, Gitman, Shishmarev 2019). Note that the corresponding limiting case of a constant uniform electric field shares many similarities with the case of the de Sitter background (see Anderson, Mottola 2014; Akhmedov, Popov 2015 and references therein). Thus, a study of the vacuum instability in the presence of the L -constant electric field with large $L \to \infty$ may be quite important for some applications. Only a critical step with a potential difference $\Delta U > 2m$ (where m is the electron mass) can produce electron-positron pairs; moreover, pairs are born only with quantum numbers in a finite range—in the so-called Klein zone.

As a matter of fact, non-perturbative calculation techniques are related to the possibility of constructing exact solutions of the corresponding relativistic Dirac and Klein-Gordon equations; for instance, solutions that have special asymptotics. Constructing such solutions is a rather difficult task. An adequate choice of variables in the corresponding equations can be useful to solve it. For instance, Narozhnyi and Nikishov (1976) found the above-mentioned solutions in a special representation considering the Dirac and Klein-Gordon equations with a constant uniform field given by time-dependent potential and choosing the variables of the light cone (see also Gavrilov, Gitman, Shvartsman 1979; Gavrilov, Gitman, Gonçalves 1998). These solutions make it possible to explicitly find all kinds of the corresponding QED singular functions in the Fock-Schwinger proper time representation. This present article uses a non-commutative integration method of linear differential equations to consider the Klein-Gordon equation with the L -constant electric field with a large L and uses the light cone variables to find new complete sets of its nonstationary exact solutions. These solutions can be related by integral transformations to previously known stationary solutions that were found by Gavrilov and Gitman (2016b). Then, the general theory developed by Gavrilov and Gitman (2016a) is used to construct—in terms of the new nonstationary solutions—the so-called in- and out-states of scalar particles confined between two capacitor plates.

In- and out-solutions

Let us construct in- and out-solutions of the Klein-Gordon equation with an external constant electric field, which is the so-called L -constant electric field and belongs to the class of x-potential steps. The equation has the form

$$\left(P^\mu P_\mu - m\right)\psi(X) = 0, \ P_\mu = i\partial_\mu - qA_\mu(X),$$
$$P^\mu = \eta^{\mu\nu}P_\nu, \ \eta^{\mu\nu} = \mathrm{diag}\underbrace{(1, -1, \dots, -1)}_{d}, \ d = D + 1, \tag{1}$$

where $A_\mu(X)$ are corresponding electromagnetic potentials, m is the particle mass and $q = -e$, $e > 0$ is its charge. For the purpose of generality, the problem is considered in d -dimensional spacetime ($\hbar = c = 1$). Here $X = (X^\mu) = (t, \mathbf{r})$, $\mathbf{r} = (X^k)$, $\mu = 0, 1, \dots D$, $k = 1, \dots, D$. The L -constant electric field $E(x)$ has the form

$$E(x) = \begin{cases} 0, & x \in (-\infty, -L/2] \cup [L/2, \infty) \\ E, & x \in (-L/2, L/2) \end{cases}, \quad L > 0. \tag{2}$$

We assume that the corresponding x-potential step is critical and sufficiently large, so that $eEL \gg 2m$. In this case, the field $E(x)$ and the leading contributions to the vacuum mean values can be considered as macroscopic ones. However, this L-constant electric field is weakly inhomogeneous, the corresponding Klein zone is extensive, so that all the universal properties of the vacuum instability described by Gavrilov, Gitman and Shishmarev (2019) hold true. The L-constant field in the limit $L \to \infty$ is a kind of a regularisation for a constant uniform electric field. In fact, the L-constant field may be approximated in this limit by a constant uniform electric field given by a linear potential

$$A_0(X) = -Ex, \quad A_k(X) = 0, \quad x = X^1, \quad E > 0. \tag{3}$$

Consider stationary solutions of the Klein-Gordon equation with the following form:

$$\psi_n(X) = \varphi_n(t, x)\varphi_{\mathbf{p}_\perp}(\mathbf{r}_\perp), \quad \varphi_{\mathbf{p}_\perp}(\mathbf{r}_\perp) = (2\pi)^{-(d-1)/2}\exp(i\mathbf{p}_\perp\mathbf{r}_\perp),$$
$$\varphi_n(t, x) = \exp(-ip_0 t)\varphi_n(x), \quad n = (p_0, \mathbf{p}_\perp), \tag{4}$$
$$X = (t, x, \mathbf{r}_\perp), \mathbf{r}_\perp = (X^2, ..., X^D), \quad \mathbf{p}_\perp = (p^2, ..., p^D), \quad \hat{p}_x = -i\partial_x.$$

These solutions are quantum states of spinless particles with given energy p_0 and momenta $\mathbf{p}_\perp$ perpendicular to the x-direction. The functions $\varphi_n(x)$ obey the second-order differential equation

$$\{\hat{p}_x^2 - [p_0 - U(x)]^2 + \mathbf{p}_\perp^2 + m^2\}\varphi_n(x) = 0, \quad U(x) = -eA_0(x). \tag{5}$$

Let us construct two complete sets of solutions with the form (4) and denote them as $_\zeta\psi_n(X)$ and $^\zeta\psi_n(X), \zeta = \pm$ with special left and right asymptotics:

$$\hat{p}_x \, _\zeta\psi_n(X) = p^{\mathrm{L}} \, _\zeta\psi_n(X), \quad x \to -\infty,$$

$$\hat{p}_x \, ^\zeta\psi_n(X) = p^{\mathrm{R}} \, ^\zeta\psi_n(X), \quad x \to +\infty.$$

The solutions $_\zeta\psi_n(X)$ and $^\zeta\psi_n(X)$ asymptotically describe particles with given real momenta $p^{\mathrm{L/R}}$ along the x direction. The corresponding functions $\varphi_n(x)$ are denoted by $_\zeta\varphi_n(x)$ and $^\zeta\varphi_n(x)$, respectively. These functions have the asymptotics

$$_\zeta\varphi_n(x) = \, _\zeta\mathcal{N}\exp\left[i\left|p^{\mathrm{L}}\right|x\right], \quad x \to -\infty,$$

$$^\zeta\varphi_n(x) = \, ^\zeta\mathcal{N}\exp\left[i\left|p^{\mathrm{R}}\right|x\right], \quad x \to +\infty.$$

Solutions $_\zeta\psi_n(X)$ and $^\zeta\psi_n(X)$ are subjected to the following orthonormality conditions with respect to the Klein-Gordon inner product on the $x = $ const hyperplane:

$$\left(\, _\zeta\psi_n, \, _{\zeta'}\psi_{n'}\right)_x = \left(\, ^\zeta\psi_n, \, ^{\zeta'}\psi_{n'}\right)_x = \zeta\delta_{\zeta,\zeta'}\delta_{n,n'},$$
$$\delta_{n,n'} = \delta(p_0 - p_0')\delta(\mathbf{p}_\perp - \mathbf{p}_\perp'), \tag{6}$$
$$(\psi, \psi')_x = i\int \psi^*(X)(\overleftarrow{\partial}_x - \overrightarrow{\partial}_x)\psi'(X)dt d\mathbf{r}_\perp.$$

Note that for two solutions with different quantum numbers n, the inner product $(\psi, \psi')_x$ can be easily calculated as

$$\left(\psi_n, \psi'_{n'}\right)_x = \mathcal{I}\,(2\pi)^{d-1}\delta_{n,n'}, \quad \mathcal{I} = \varphi_n^*(x)\left(i\overleftarrow{\partial}_x - i\overrightarrow{\partial}_x\right)\varphi'_n(x). \tag{7}$$

Solutions ${}_\zeta\psi_n(X)$ and ${}^\zeta\psi_n(X)$ can be decomposed through each other as follows:

$$\begin{aligned}
{}^\zeta\psi_n(X) &= {}_+\psi_n(X)g\left({}_+\middle|{}^\zeta\right) - {}_-\psi_n(X)g\left({}_-\middle|{}^\zeta\right),\\
{}_\zeta\psi_n(X) &= {}^-\psi_n(X)g\left({}^-\middle|{}_\zeta\right) - {}^+\psi_n(X)g\left({}^+\middle|{}_\zeta\right),
\end{aligned} \tag{8}$$

where the expansion coefficients are defined by the equations

$$\left({}_\zeta\psi_n,\ {}^{\zeta'}\psi_{n'}\right)_x = g\left({}_\zeta\middle|{}^{\zeta'}\right)\delta_{n,n'}, \quad g\left({}^{\zeta'}\middle|{}_\zeta\right) = g\left({}_\zeta\middle|{}^{\zeta'}\right)^*.$$

Equation (5) can be written as

$$\left[\frac{\mathrm{d}^2}{\mathrm{d}\xi^2} + \xi^2 - \lambda\right]\varphi_n(x) = 0, \quad \xi = \frac{eEx - p_0}{\sqrt{eE}}, \quad \lambda = \frac{\pi_\perp^2}{eE}.$$

Its general solution can be written in terms of an appropriate pair of linearly independent Weber parabolic cylinder functions (WPCFs), either as $D_\rho[(1-\mathrm{i})\xi]$ and $D_{-1-\rho}[(1+\mathrm{i})\xi]$ or $D_\rho[-(1-\mathrm{i})\xi]$ and $D_{-1-\rho}[-(1+\mathrm{i})\xi]$, where $\rho = -\mathrm{i}\lambda/2 - 1/2$.

Using asymptotic expansions of WPCFs, the functions ${}_\zeta\varphi_n(x)$ and ${}^\zeta\varphi_n(x)$ can be constructed as

$$\begin{aligned}
{}_+\varphi_n(x) &= {}_+\mathcal{N}D_{-1-\rho}[-(1+\mathrm{i})\xi] \sim e^{-\mathrm{i}\xi^2/2}, \quad \xi \to -\infty, \; p^{\mathrm{L}} = -\xi\sqrt{eE}\\
{}_-\varphi_n(x) &= {}_-\mathcal{N}D_\rho[-(1-\mathrm{i})\xi] \sim e^{\mathrm{i}\xi^2/2}, \quad \xi \to -\infty, \; p^{\mathrm{L}} = \xi\sqrt{eE};\\
{}^+\varphi_n(x) &= {}^+\mathcal{N}D_\rho[(1-\mathrm{i})\xi] \sim e^{\mathrm{i}\xi^2/2}, \quad \xi \to \infty, \; p^{\mathrm{R}} = \xi\sqrt{eE},\\
{}^-\varphi_n(x) &= {}^-\mathcal{N}D_{-1-\rho}[(1+\mathrm{i})\xi] \sim e^{-\mathrm{i}\xi^2/2}, \quad \xi \to \infty, \; p^{\mathrm{R}} = -\xi\sqrt{eE},
\end{aligned} \tag{9}$$

$$\quad {}_\zeta\mathcal{N} = {}^\zeta\mathcal{N} = (2eE)^{-1/4}e^{\pi\lambda/8}. \tag{10}$$

Their in- and out-classifications are related to the signs of the asymptotic momenta p^{L} and p^{R} (see Gavrilov, Gitman 2016b). Namely,
${}_+\psi_n, {}^+\psi_n$ are in-states and ${}_-\psi_n, {}^-\psi_n$ are out-states.

It is useful to construct two different complete sets of solutions of the Klein-Gordon equation (1) that are not stationary states and can be written as

$$\psi_\sigma(X) = \varphi_\sigma(t, x)\varphi_{\mathbf{p}_\perp}(\mathbf{r}_\perp), \tag{11}$$

where σ is a set of quantum numbers that will be defined below. In this case, the function $\varphi_\sigma(t, x)$ satisfies the equation

$$\{\hat{p}_x^2 - [\hat{p}_0 - U(x)]^2 + \mathbf{p}_\perp^2 + m^2\}\varphi_\sigma(t, x) = 0, \quad \hat{p}_0 = \mathrm{i}\partial_t. \tag{12}$$

This equation admits integrals of motion in the class of linear differential operators of the first order, which are

$$\hat{Y}_0 = -\mathrm{i}e, \quad \hat{Y}_1 = \partial_t, \quad \hat{Y}_2 = \partial_x + \mathrm{i}eEt, \quad \hat{Y}_3 = x\partial_t + t\partial_x + \frac{\mathrm{i}eE}{2}(t^2 + x^2).$$

The operators $\hat{Y}_a$, $a = 0,1,2,3$ form a four-dimensional Lie algebra $\mathfrak{g}$ with nonzero commutation relations

$$\left[\hat{Y}_1, \hat{Y}_2\right] = -E\,\hat{Y}_0, \quad [\hat{Y}_1, \hat{Y}_3] = \hat{Y}_2, \quad [\hat{Y}_2, \hat{Y}_3] = \hat{Y}_1.$$

Equation (12) can be considered as an equation for the eigenfunctions of the Casimir operator $K(-i\hat{Y}) = -2E\,\hat{Y}_0\hat{Y}_3 + \hat{Y}_1^2 - \hat{Y}_2^2$,

$$-K(-i\hat{Y})\varphi_\sigma(t, x) = (\mathbf{p}_\perp^2 + m^2)\varphi_\sigma(t, x).$$

At this stage, we follow a non-commutative integration method of linear differential equations (Shapovalov, Shirokov 1995; Bagrov, Baldiotti, Gitman et al. 2002; Breev, Shapovalov 2016), which allows us to construct a complete set of solutions based on a symmetry of the equation. An irreducible representation of the Lie algebra $\mathfrak{g}$ in the space of functions of the variable $\tilde{p} \in (-\infty, +\infty)$ is defined by the help of the operators $\ell_a(\tilde{p}, \partial_{\tilde{p}}, j)$:

$$\ell_0(\tilde{p}, \partial_{\tilde{p}}, j) = ie, \quad \ell_1(\tilde{p}, \partial_{\tilde{p}}, j) = -eE\partial_{\tilde{p}} + \frac{i}{2}\tilde{p},$$

$$\ell_2(\tilde{p}, \partial_{\tilde{p}}, j) = eE\partial_{\tilde{p}} + \frac{i}{2}\tilde{p}, \quad \ell_3(\tilde{p}, \partial_{\tilde{p}}, j) = -\tilde{p}\partial_{\tilde{p}} + ij - \frac{1}{2}, \quad j > 0,$$

where j parameterises the non-degenerate adjoint orbits of a Lie algebra $\mathfrak{g}$. The following relations hold true:

$$[\ell_1, \ell_2] = -E\,\ell_0, \quad [\ell_1, \ell_3] = \ell_2, \quad [\ell_2, \ell_3] = \ell_1,$$

$$K(-i\ell(\tilde{p}, \partial_{\tilde{p}}, j)) = (2eE)j.$$

Integrating the equations

$$\left[\hat{Y}_a + \ell_a(\tilde{p}, \partial_{\tilde{p}}, j)\right]\varphi_\sigma(t, x) = 0 \tag{13}$$

together with the equation (5), we fix $j = -\lambda/2$ and derive a set of solutions which is characterised by quantum numbers $\sigma = (\tilde{p}, \mathbf{p}_\perp)$,

$$\begin{aligned}&{}^+_-\varphi_\sigma(t, x) = {}^+_-C_\sigma \exp\left(ie\frac{E}{2}\left[\frac{1}{2}x_-^2 - t^2\right] - \frac{i}{2}[\lambda - i]\left(\ln\frac{\pm i\pi_-}{\sqrt{eE}}\right) - \frac{i}{2}\tilde{p}\,x_+\right),\\&\pi_- = \tilde{p} + eEx_-, \quad x_\pm = t \pm x.\end{aligned} \tag{14}$$

The parameter $\tilde{p}$ is an eigenvalue of the symmetry operator $i(\hat{Y}_1 + \hat{Y}_2)$:

$$i(\hat{Y}_1 + \hat{Y}_2)\,{}^+_-\varphi_\sigma(t, x) = \tilde{p}\,{}^+_-\varphi_\sigma(t, x).$$

It is possible to interpret the quantum numbers σ from the perspective of the orbit method: the parameter $\lambda = (m^2 + \mathbf{p}_\perp^2)/(eE)$ describes the Casimir operator $K(-i\hat{Y})$ spectrum and parameterises the non-degenerate orbits of the co-adjoint representation of the local Lie group $\exp\mathfrak{g}$ (in this case, the orbits are hyperbolic paraboloids), and the variation region of the parameter $\tilde{p}$ is a Lagrangian submanifold to these orbits.

In order to classify solutions (11), we define direct and inverse integral transformations that relate these solutions to solutions (4), which are stationary states, eigenfunctions for the operator $\hat{p}_0$.

We represent solutions of both equation (5) and

$$\hat{p}_0\,\varphi_n^{(\pm)}(t, x) = p_0\,\varphi_n^{(\pm)}(t, x)$$

in the following form

$$\varphi_n^{(\pm)}(t,x) = (2\pi eE)^{-1/2} \int_{-\infty}^{+\infty} M^*(p_0,\tilde{p}) \, {}^{\pm}_{-}\varphi_\sigma(t,x) dp. \tag{15}$$

Taking into account condition (13), the equation for the function $M(p_0,\tilde{p})$ can be written as:

$$-i\ell_1(\tilde{p}, \partial_{\tilde{p}}, j) M(p_0,\tilde{p}) = p_0 M(p_0,\tilde{p}).$$

We choose its particular solution

$$M(p_0,\tilde{p}) = \exp\left(\frac{i}{4eE}[\tilde{p}^2 - 4\tilde{p}p_0]\right), \tag{16}$$

which satisfies the orthogonality relation

$$\int_{-\infty}^{+\infty} M^*(p_0,\tilde{p}) M(p_0,\tilde{p}') dp_0 = 2\pi eE \, \delta(\tilde{p} - \tilde{p}'). \tag{17}$$

The inverse to (15) transformation reads:

$${}^{+}_{-}\varphi_\sigma(t,x) = (2\pi eE)^{-1/2} \int_{-\infty}^{+\infty} M(p_0,\tilde{p}) \varphi_n^{(\pm)}(t,x) dp_0. \tag{18}$$

Thus, direct (15) and inverse (18) integral transformation were defined with kernel (16) that converts solutions (14) into solutions that are eigenfunctions for the operator $\hat{p}_0$. Applying one of the integral transformations to solutions (14), we get:

$$\varphi_n^{(\pm)}(t,x) = (2\pi eE)^{-\frac{1}{2}} \int_{-\infty}^{+\infty} M^*(p_0,\tilde{p}) {}^{\pm}_{-}\varphi_\sigma(t,x) d\tilde{p} =$$
$$= {}^{\pm}_{-}C_\sigma(1-i)^{\rho+1} e^{\frac{ip_0^2}{2eE}} e^{-ip_0 t} D_\rho[\pm(1-i)\xi]. \tag{19}$$

Then, comparing the equation (19) with the equations (9)-(10) gives the following correspondence:

$$\varphi_n^{(+)}(t,x) \sim {}^{+}\mathcal{N}' e^{-ip_0 t} D_\rho[+(1-i)\xi] = {}^{+}\varphi_n(x) e^{-ip_0 t},$$
$$\varphi_n^{(-)}(t,x) \sim {}_{-}\mathcal{N}' e^{-ip_0 t} D_\rho[-(1-i)\xi] = {}_{-}\varphi_n(x) e^{-ip_0 t}. \tag{20}$$

Transformation (18) makes it possible to derive orthonormality relations on the hyperplane $x = \mathrm{const}$ for scalar particles constructing with the help of functions ${}^{+}_{-}\varphi_\sigma(t,x)$,

$$({}^{+}_{-}\psi_\sigma, {}^{+}_{-}\psi_{\sigma'})_x = \pm\delta_{\sigma,\sigma'}, \tag{21}$$

where

$${}^{+}_{-}\psi_\sigma(X) = {}^{+}_{-}\varphi_\sigma(t,x)\varphi_{\mathbf{p}_\perp}(\mathbf{r}_\perp), \tag{22}$$

and determine the normalising factors ${}^{+}_{-}C_\sigma$,

$${}^{+}_{-}C_\sigma = \frac{1}{\sqrt{4\pi eE}} e^{\pi\lambda/4}.$$

Thus, we obtain:

$$({}_{-}\psi_\sigma, {}^{+}\psi_{\sigma'})_x = g({}_{-}|{}^{+})\delta_{\sigma,\sigma'}, \quad g({}_{-}|{}^{+}) = ie^{\pi\lambda/2}.$$

Let us introduce the following notation:

$$\varphi_n^{(\pm)}(t, x) = {}^{\pm}_{-}\varphi_n(x)\exp(-ip_0t), \ {}^{\pm}_{-}\psi_n(X) = \varphi_n^{(\pm)}(t, x)\varphi_{\mathbf{p}_\perp}(\mathbf{r}_\perp).$$

It follows from (15) and (18) that

$$\begin{aligned}
{}^{\pm}_{-}\psi_\sigma(X) &= (2\pi eE)^{-1/2} \int_{-\infty}^{+\infty} M(p_0, \tilde{p}) \, {}^{\pm}_{-}\psi_n(X) dp_0, \\
{}^{\pm}_{-}\psi_n(X) &= (2\pi eE)^{-1/2} \int_{-\infty}^{+\infty} M^*(p_0, \tilde{p}) \, {}^{\pm}_{-}\psi_\sigma(X) d\tilde{p}.
\end{aligned} \tag{23}$$

Let us consider another type of solutions:

$$\begin{aligned}
{}_{+}\varphi_\sigma(t, x) &= \theta(-\pi_-) \, {}^{+}\varphi_\sigma(t, x), \\
{}^{-}\varphi_\sigma(t, x) &= \theta(+\pi_-) \, {}_{-}\varphi_\sigma(t, x).
\end{aligned} \tag{24}$$

The corresponding integral transformation is

$$\begin{aligned}
{}_{+}\varphi_n(t, x) &= (2\pi eE)^{-\frac{1}{2}} \int_{-\infty}^{+\infty} M^*(p_0, \tilde{p})\theta(-\pi_-) \, {}^{+}\varphi_\sigma(t, x) d\tilde{p} = \\
&= - \, {}^{+}C_\sigma \sqrt{\frac{2}{\pi}} (-[1 + i])^{\rho-1} \, \Gamma(\rho + 1) e^{\frac{ip_0^2}{2eE}} e^{-ip_0t} D_{-\rho-1}[-(1 + i)\xi] \\
{}^{-}\varphi_n(t, x) &= (2\pi eE)^{-\frac{1}{2}} \int_{-\infty}^{+\infty} M^*(p_0, \tilde{p})\theta(\pi_-) \, {}_{-}\varphi_\sigma(t, x) d\tilde{p} = \\
&= - \, {}_{-}C_\sigma \sqrt{\frac{2}{\pi}} (-[1 + i])^{\rho-1} \, \Gamma(\rho + 1) e^{\frac{ip_0^2}{2eE}} e^{-ip_0t} D_{-\rho-1}[(1 + i)\xi],
\end{aligned} \tag{25}$$

so that

$$\begin{aligned}
{}_{+}\varphi_n(t, x) &\sim \, {}_{+}\mathcal{N}' e^{-ip_0t} D_{-1-\rho}[-(1 + i)\xi] = \, {}_{+}\varphi_n(x)e^{-ip_0t}, \\
{}^{-}\varphi_n(t, x) &\sim \, {}^{-}\mathcal{N}' e^{-ip_0t} D_{-1-\rho}[(1 + i)\xi] = \, {}^{-}\varphi_n(x)e^{-ip_0t}.
\end{aligned} \tag{26}$$

Using functions ${}^{-}_{+}\varphi_\sigma(t, x)$, we construct a new set of solutions

$${}^{-}_{+}\psi_\sigma(t, x)(X) = \sqrt{e^{\pi\lambda} - 1} \, {}^{-}_{+}\varphi_\sigma(t, x)\varphi_{\mathbf{p}_\perp}(\mathbf{r}_\perp), \tag{27}$$

which satisfies the following orthonormality relations:

$$({}_{+}\psi_\sigma, {}_{-}\psi_{\sigma'})_x = 0, \ ({}^{-}\psi_\sigma, {}^{+}\psi_{\sigma'})_x = 0, \ ({}^{-}_{+}\psi_\sigma, {}^{-}_{+}\psi_\sigma)_x = \pm\delta_{\sigma,\sigma'}.$$

Based on (25) and (17), the integral transformations are

$$\begin{aligned}
{}^{-}_{+}\psi_\sigma(X) &= (2\pi eE)^{-1/2} \int_{-\infty}^{+\infty} M(p_0, \tilde{p}) \, {}^{-}_{+}\psi_n(X) dp_0, \\
{}^{-}_{+}\psi_n(X) &= (2\pi eE)^{-1/2} \int_{-\infty}^{+\infty} M^*(p_0, \tilde{p}) \, {}^{-}_{+}\psi_\sigma(X) d\tilde{p}.
\end{aligned} \tag{28}$$

There exist useful relations between solutions ${}_\zeta\psi_\sigma(X)$ and ${}^\zeta\psi_\sigma(X)$. Each of them is complete for a given σ and can be decomposed through another one as follows:

$$
\begin{aligned}
{}^\zeta\psi_\sigma(X) &= {}_+\psi_\sigma(X)g({}_+|{}^\zeta) - {}_-\psi_\sigma(X)g({}_-|{}^\zeta), \\
{}_\zeta\psi_\sigma(X) &= {}^-\psi_\sigma(X)g({}^-|{}_\zeta) - {}^+\psi_\sigma(X)g({}^+|{}_\zeta),
\end{aligned}
\tag{29}
$$

Equations

$$
\left({}_\zeta\psi_\sigma, {}^{\zeta'}\psi_{\sigma'}\right)_x = g({}_\zeta|{}^{\zeta'})\delta_{\sigma,\sigma'}, \quad g({}^{\zeta'}|{}_\zeta) = g({}_\zeta|{}^{\zeta'})^*
$$

allow us to calculate coefficients $g({}_-|{}^-)$ and $g({}_+|{}^+)$,

$$
g({}^-|{}_-) = -\sqrt{e^{\pi\lambda} - 1}, \quad g({}^+|{}_+) = +\sqrt{e^{\pi\lambda} - 1}.
$$

We note that the relations (29) are similar to the relations (8) that were established for the solutions ${}_\zeta\psi_n(X)$ and ${}^\zeta\psi_n(X)$ (in this case, the coefficients g do not depend on p_0 and $\tilde{p}$). From (20) and (26) it follows that ${}_+\psi_n$, ${}^+\psi_n$ are in-states and ${}_-\psi_n$, ${}^-\psi_n$ are out-states.

From the equation (24) it follows that

$$
\begin{aligned}
{}_+\psi_\sigma(X) &= 0, \quad \pi_- > 0, \\
{}^-\psi_\sigma(X) &= 0, \quad \pi_- < 0.
\end{aligned}
\tag{30}
$$

Then, taking into account equations (29) and (30), we get:

$$
\begin{aligned}
{}_+\psi_\sigma(X) &= g({}_+|{}^-)^{-1}[{}_-\psi_\sigma(X)g({}_-|{}^-) + \\
&\quad + {}^-\psi_\sigma(X)] = 0, \quad \pi_- > 0, \\
{}^-\psi_\sigma(X) &= g({}^-|{}_+)^{-1}[{}^+\psi_\sigma(X)g({}^+|{}_+) + \\
&\quad + {}_+\psi_\sigma(X)] = 0, \quad \pi_- < 0.
\end{aligned}
\tag{31}
$$

Since the coefficient $g({}_+|{}^-)$ is not zero for all σ, the equations (31) imply a direct connection between the solutions ${}_\zeta\psi_\sigma(X)$ and ${}^\zeta\psi_\sigma(X)$ normalised on the hyperplane $x = \text{const}$,

$$
\begin{aligned}
{}^-\psi_\sigma(X) &= -{}_-\psi_\sigma(X)g({}_-|{}^-)\theta(\pi_-), \\
{}_+\psi_\sigma(X) &= -{}^+\psi_\sigma(X)g({}^+|{}_+)\theta(-\pi_-).
\end{aligned}
$$

Thus, using the non-commutative integration method for the equation (12), we obtained in- and out-states of scalar particles in terms of new solutions (22) and (27), which are non-stationary and are determined by a set of quantum numbers σ. Solutions $\{{}_+\psi_\sigma, {}^+\psi_\sigma\}$ describe in-states and solutions $\{{}_-\psi_\sigma, {}^-\psi_\sigma\}$ describe out-states. It follows from the integral transformations (23) and (28) that the solutions ${}_\zeta\psi_\sigma(X)$ and ${}^\zeta\psi_\sigma(X)$ are related to the well-known stationary solutions ${}_\zeta\psi_n(X)$ and ${}^\zeta\psi_n(X)$ (see Gavrilov, Gitman 2016b).

References

Akal, I., Egger, R., Müller, C., Villalba-Chávez, S. (2019) Simulating dynamically assisted production of Dirac pairs in gapped graphene monolayers. *Physical Review D*, 99 (1), 016025. DOI: 10.1103/PhysRevD.99.016025 (In English)

Akhmedov, E. T., Popov, F. K. (2015) A few more comments on secularly growing loop corrections in strong electric fields. *Journal of High Energy Physics*, 9, 85. DOI: 10.1007/JHEP09(2015)085 (In English)

Allor, D., Cohen, T. D., McGady, D. A. (2008) Schwinger mechanism and graphene. *Physical Review D*, 78 (9), 096009. DOI: 10.1103/PhysRevD.78.096009 (In English)

Anderson, P. R., Mottola, E. (2014) Instability of global de Sitter space to particle creation. *Physical Review D*, 89 (10), 104038. DOI: 10.1103/PhysRevD.89.104038 (In English)

Bagrov, V. G., Baldiotti, M. C., Gitman, D. M., Shirokov, I. V. (2002) New solutions of relativistic wave equations in magnetic fields and longitudinal fields. *Journal of Mathematical Physics*, 43, 2284. DOI: 10.1063/1.1461428 (In English)

Breev, A. I., Shapovalov, A. V. (2016) The Dirac equation in an external electromagnetic field: Symmetry algebra and exact integration. *Journal of Physics: Conference Series*, 670, 012015. DOI: 10.1088/1742-6596/670/1/012015 (In English)

Das Sarma, S., Adam, S., Hwang, E. H., Rossi, E. (2011) Electronic transport in two-dimensional graphene. *Reviews of Modern Physics*, 83 (2), 407. DOI: 10.1103/RevModPhys.83.407 (In English)

Di Piazza, A., Müller, C., Hatsagortsyan, K. Z., Keitel, C. H. (2012) Extremely high-intensity laser interactions with fundamental quantum systems. *Reviews of Modern Physics*, 84 (3), 1177. DOI: 10.1103/RevModPhys.84.1177 (In English)

Dunne, G. V. (2009) New strong-field QED effects at extreme light infrastructure. *The European Physical Journal D*, 55 (2), 327. DOI: 10.1140/epjd/e2009-00022-0 (In English)

Dunne, G. V. (2014) Extreme quantum field theory and particle physics with IZEST. *The European Physical Journal Special Topics*, 223 (6), 1055–1061. DOI: 10.1140/epjst/e2014-02156-4 (In English)

Fradkin, E. S., Gitman, D. M. (1981) Furry picture for quantum electrodynamics with pair-creating external field. *Fortschritte der Physik — Progress of Physics*, 29 (9), 381–411. DOI: 10.1002/prop.19810290902 (In English)

Fradkin, E. S., Gitman, D. M., Shvartsman, S. M. (1991) *Quantum electrodynamics with unstable vacuum*. Berlin: Springer, 288 p. (In English)

Gavrilov, S. P., Gitman, D. M. (2016a) Quantization of charged fields in the presence of critical potential steps. *Physical Review D*, 93 (4), 045002. DOI: 10.1103/PhysRevD.93.045002 (In English)

Gavrilov, S. P., Gitman, D. M. (2016b) Scattering and pair creation by a constant electric field between two capacitor plates. *Physical Review D*, 93 (4), 045033. DOI: 10.1103/PhysRevD.93.045033 (In English)

Gavrilov, S. P., Gitman, D. M., Gonçalves, A. E. (1998) QED in external field with space-time uniform invariants: Exact solutions. *Journal of Mathematical Physics*, 39 (7), 3547. DOI: 10.1063/1.532451 (In English)

Gavrilov, S. P., Gitman, D. M., Shishmarev, A. A. (2017) Particle scattering and vacuum instability by exponential steps. *Physical Review D*, 96 (9), 096020. DOI: 10.1103/PhysRevD.96.096020 (In English)

Gavrilov, S. P., Gitman, D. M., Shishmarev, A. A. (2019) Pair production from the vacuum by a weakly inhomogeneous space-dependent electric potential. *Physical Review D*, 99 (11), 116014. DOI: 10.1103/PhysRevD.99.116014 (In English)

Gavrilov, S. P., Gitman, D. M., Shvartsman, Sh. M. (1979) Green's functions in an external electric field. *Soviet Journal of Nuclear Physics*, 29, 567–572. (In English)

Gavrilov, S. P., Gitman, D. M., Yokomizo, N. (2012) Dirac fermions in strong electric field and quantum transport in graphene. *Physical Review D*, 86 (12), 125022. DOI: 10.1103/PhysRevD.86.125022 (In English)

Gelis, F., Tanji, N. (2016) Schwinger mechanism revisited. *Progress in Particle and Nuclear Physics*, 87, 1–49. DOI: 10.1016/j.ppnp.2015.11.001 (In English)

Gitman, D. M. (1977) Processes of arbitrary order in quantum electrodynamics with a pair-creating external field. *Journal of Physics A: Mathematical and General*, 10 (11), 2007–2020. DOI: 10.1088/0305-4470/10/11/026 (In English)

Hegelich, B. M., Mourou, G., Rafelski, J. (2014) Probing the quantum vacuum with ultra-intense laser pulses. *The European Physical Journal Special Topics*, 223 (6), 1093–1104. DOI: 10.1140/epjst/e2014-02160-8 (In English)

Kané, G., Lazzeri, M., Mauri, F. (2015) High-field transport in graphene: The impact of Zener tunneling. *Journal of Physics: Condensed Matter*, 27 (16), 164205. DOI: 10.1088/0953-8984/27/16/164205 (In English)

Mourou, G., Tajima, T. (2014) Summary of the IZEST science and aspiration. *The European Physical Journal Special Topics*, 223 (6), 979–984. DOI: 10.1140/epjst/e2014-02148-4 (In English)

Narozhnyi, N. B., Nikishov, A. I. (1976) Solutions of the Klein-Gordon and Dirac equations for a particle in a constant electric field and a plane electromagnetic wave propagating along the field. *Theoretical and Mathematical Physics*, 26 (1), 9–20. DOI: 10.1007/BF01038251 (In English)

Oladyshkin, I. V., Bodrov, S. B., Sergeev, Yu. A. et al. (2017) Optical emission of graphene and electron-hole pair production induced by a strong terahertz field. *Physical Review B*, 96 (15), 155401. DOI: 10.1103/PhysRevB.96.155401 (In English)

Ruffini, R., Vereshchagin, G., Xue, S.-S. (2010) Electron–positron pairs in physics and astrophysics: From heavy nuclei to black holes. *Physics Reports*, 487 (1–4), 1–140. DOI: 10.1016/j.physrep.2009.10.004 (In English)

Schwinger, J. (1951) On gauge invariance and vacuum polarization. *Physical Review*, 82 (5), 664. DOI: 10.1103/PhysRev.82.664 (In English)

Shapovalov, A. V., Shirokov, I. V. (1995) Noncommutative integration of linear differential equations. *Theoretical and Mathematical Physics*, 104 (2), 921–934. DOI: 10.1007/BF02065973 (In English)

Vafek, O., Vishwanath, A. (2014) Dirac fermions in solids: From high- cuprates and graphene to topological insulators and Weyl semimetals. *Annual Review of Condensed Matter Physics*, 5 (1), 83–112. DOI: 10.1146/annurev-conmatphys-031113-133841 (In English)

UDC 524.8

Rotating black holes as sources of high energy particles

A. A. Grib[⊠1], Y. V. Pavlov[2]

[1] Herzen State Pedagogical University of Russia, 48 Moika River Emb., Saint Petersburg 191186, Russia
[2] Institute for Problems of Mechanical Engineering RAS, 61 Bolshoj Prosp. V. O.,
Saint Petersburg 199178, Russia

Authors

Andrey A. Grib, ORCID: 0000-0002-6389-991X, e-mail: andrei_grib@mail.ru

Yurii V. Pavlov

Abstract. Ultrahigh energy particles in cosmic rays observed on the Earth can have their origin in the ergosphere of rotating black holes. This paper discusses production of these particles through decay of superheavy dark matter particles, such as multiparticle scattering near horizon, as well as a collision of particles with a large angular momentum and particles on white hole geodesics.

Keywords: rotating black hole, Kerr metric, ergosphere, particle collisions.

Introduction

Dark matter is one of the major questions of modern physics. Astronomical observations show that only five percent of matter is composed of visible matter, mainly protons, electrons and photons of the background radiation, while 69 percent is dark energy and 26 percent is composed of dark matter. The main hypothesis is that dark matter particles are weakly interacting massive particles (WIMP).

Grib and Pavlov (2002a; 2002b) formulated a hypothesis that dark matter particles are neutral scalar particles with the mass of the grand unification scale. Their mass is derived from the calculations of particle creation from vacuum by the strong gravitation field of the early universe. These calculations showed that the number of created particles with this mass equals the Eddington number—the number of visible particles (Grib, Mamayev, Mostepanenko 1994).

Thus, if the created particles later decayed into visible particles when the temperature of the universe was high, while some part of them survived at lower temperatures as dark matter particles, it explains both the number of visible particles and also the closeness of the visible particle density and the dark matter density (Grib, Pavlov 2008b).

This GP hypothesis (Grib, Pavlov 2008b) can be proved by indirect observation of a similar process, the decay of superheavy dark matter particles into usual particles at high energies. At low energies dark matter particles are stable. In cosmic rays, particles with high energies up to 1020 eV are observed (Aab, Abreu, Aglietta et al. 2017). They are called ultra high energy cosmic rays (UHECR). The main hypothesis of their origin is that they are produced in Active Galactic Nuclei (AGN). AGN are considered to be rotating black holes. General relativity gives the description of AGN in terms of the Kerr metric. Piran,

Katz and Shaham (Piran, Shaham, Katz 1975) and Bañados, Silk and West (Bañados, Silk, West 2009) discovered that very high energies can be obtained in the process of particle collisions in the vicinity of the rotating black hole's horizon, or the so-called ergosphere. Thus, a black hole plays the role of a natural collider with energies much higher than those in the Large Hadron Collider (LHC) on the Earth. They can be of the grand unification scale and even of the Planck energy scale. However, it is possible to conclude that ergosphere processes taking place in the early universe, i.e. the decays of dark matter into usual particles, are still present (Grib, Pavlov 2008a; 2009). The products of these decays reach the Earth and are observed as UHECR. This paper presents an overview of the results obtained in the previous papers (Grib, Pavlov 2010; 2011; Grib, Pavlov, Piattella 2012; Grib, Pavlov 2013a; 2013b; 2015a; 2015b).

The structure of this paper is as follows. The first part presents basic notions for the description of rotating black holes in terms of general relativity. The second part discusses the Banados-Silk-West effect (the BSW effect) for extremal black holes and the GP effect—getting very high energies in the centre of mass frame—for nonextremal black holes. The possibility of getting high energy due to the large angular momentum of a particle is discussed in the third part. The fourth part considers the role of the "white hole" geodesics in the ergosphere. The conclusion provides a summary of research results.

The paper uses the system of units $G = c = 1$ for the gravitational constant and the speed of light.

Kerr metric and geodesics

The Kerr metric of the rotating black hole (Kerr 1963) in the Boyer-Lindquist coordinates (Boyer, Lindquist 1967) is

$$ds^2 = \frac{\rho^2 \Delta}{\Sigma^2} dt^2 - \frac{\sin^2\theta}{\rho^2} \Sigma^2 (d\varphi - \omega dt)^2 - \frac{\rho^2}{\Delta} dr^2 - \rho^2 d\theta^2, \tag{1}$$

where

$$\rho^2 = r^2 + a^2 \cos^2\theta, \quad \Delta = r^2 - 2Mr + a^2, \tag{2}$$

$$\Sigma^2 = (r^2 + a^2)^2 - a^2 \sin^2\theta \Delta, \quad \omega = \frac{2Mra}{\Sigma^2}, \tag{3}$$

M is the mass of the black hole, aM is the angular momentum. Supposing that $0 \le a \le M$, the event horizon for the Kerr black hole is given by

$$r = r_H \equiv M + \sqrt{M^2 - a^2}. \tag{4}$$

The surface

$$r = r_C \equiv M - \sqrt{M^2 - a^2} \tag{5}$$

is the Cauchy horizon. The surface of the static limit is defined by

$$r = r_1 \equiv M + \sqrt{M^2 - a^2 \cos^2\theta}. \tag{6}$$

The region of the space-time between the static limit and the event horizon is called ergosphere (Misner, Thorne, Wheeler 1973; Frolov, Novikov 2012). On the frontier of the ergosphere the function

$$S(r, \theta) = r^2 - 2Mr + a^2 \cos^2\theta \tag{7}$$

is zero, while inside the ergosphere it is $S(r, \theta) < 0$.

The geodesics equations for the Kerr metric (1) (Chandrasekhar 1983; Frolov, Novikov 2012) are

$$\rho^2 \frac{dt}{d\lambda} = \frac{1}{\Delta}\left(\Sigma^2 E - 2MraJ\right), \quad \rho^2 \frac{d\varphi}{d\lambda} = \frac{1}{\Delta}\left(2MraE + \frac{SJ}{\sin^2\theta}\right), \tag{8}$$

$$\rho^2 \frac{dr}{d\lambda} = \sigma_r \sqrt{R}, \qquad \rho^2 \frac{d\theta}{d\lambda} = \sigma_\theta \sqrt{\Theta}, \tag{9}$$

$$R = \Sigma^2 E^2 - \frac{SJ^2}{\sin^2\theta} - 4MraEJ - \Delta\left[m^2\rho^2 + \Theta\right], \tag{10}$$

$$\Theta = Q - \cos^2\theta\left[a^2(m^2 - E^2) + \frac{J^2}{\sin^2\theta}\right]. \tag{11}$$

Here $E = const$ is the energy (relative to infinity) of the moving particle, J is the conserved angular momentum projection on the rotation axis, m is the rest mass of the particle, λ is the affine parameter along the geodesic. For the particle with $m \neq 0$, the parameter $\lambda = \tau / m$, where τ is the proper time. Q is the Carter constant. $Q = 0$ for the movement in the equatorial plane $(\theta = \pi / 2)$. The constants $\sigma_r, \sigma_\theta = \pm 1$ define the direction of movement in coordinates r, θ.

It follows from (9) that the parameters characterising any geodesic must satisfy the conditions

$$R \geq 0, \qquad \Theta \geq 0. \tag{12}$$

The geodesic being the trajectory of the test particle moving outside the event horizon requires the "forward in time" movement

$$dt / d\lambda > 0. \tag{13}$$

The conditions (12) and (13) lead to inequalities in possible values of the energy E and the angular momentum projection J of the test particle at the point with coordinates (r, θ) with fixed value $\Theta \geq 0$ (Grib, Pavlov 2013b).

Outside the ergosphere $S(r, \theta) > 0$,

$$E \geq \frac{1}{\rho^2}\sqrt{(m^2\rho^2 + \Theta)S}, \quad J \in \left[J_-(r, \theta), J_+(r, \theta)\right], \tag{14}$$

$$J_\pm(r, \theta) = \frac{\sin\theta}{S}\left[-2rMaE\sin\theta \pm \sqrt{\Delta\left(\rho^4 E^2 - (m^2\rho^2 + \Theta)S\right)}\right]. \tag{15}$$

On the frontier of the ergosphere (for $\theta \neq 0, \pi$)

$$r = r_1(\theta) \implies E \geq 0, \quad J \leq E\left[\frac{Mr_1(\theta)}{a} + a\sin^2\theta\left(1 - \frac{m^2}{2E^2} - \frac{\Theta}{4Mr_1(\theta)E^2}\right)\right]. \tag{16}$$

The value $E = 0$ is possible on the frontier of the ergosphere when $m = 0$, $\Theta = 0$. In this case, any value of $J < 0$ is possible.

Inside the ergosphere $r_H < r < r_1(\theta)$, $S < 0$

$$J \leq \frac{\sin\theta}{-S}\left[2rMaE\sin\theta - \sqrt{\Delta\left(\rho^4 E^2 - (m^2\rho^2 + \Theta)S\right)}\right] \tag{17}$$

and the energy of the particle, as it is known, can be either positive or negative.

According to (16) and (17), the angular momentum projection of the particles moving along geodesics for the fixed value of the energy can be negative on the frontier and inside the ergosphere and its absolute value number can be infinitely large. This property was first found by Grib, Pavlov (2013a; 2013b) for the Kerr metric and, as Zaslavskii (2013) showed later, it is valid in the ergosphere of any black hole with an axially symmetric metric.

Note that in the vicinity of the horizon (17) has the form

$$J(r) \leq J_H = \frac{2r_H ME}{a}, \quad r \to r_H. \tag{18}$$

BSW-effect and multiparticle scattering

Energy in the centre of the mass frame $E_{c.m.}$ of two colliding particles with rest masses m_1 and m_2 is found by squaring the formula

$$\left(E_{c.m.},0,0,0\right) = p^i_{(1)} + p^i_{(2)},$$ (19)

where $p^i_{(n)}$ means four-momenta of particles $(n=1,2)$. Due to $p^i_{(n)}p_{(n)i} = m^2_n$, one has

$$E^2_{c.m.} = m^2_1 + m^2_2 + 2p^i_{(1)}p_{(2)i}.$$ (20)

Consider the collision of two massive particles. For massive particles $p^i_{(n)} = m_{(n)}u^i_{(n)}$, where $u^i = dx^i/d\tau$. In this case, as seen from (20), the energy $E_{c.m.}$ has the maximal value for given $u_{(1)}, u_{(2)}$ and $m_1 + m_2$, if the particle masses are equal: $m_1 = m_2$.

Let us find the expression of the energy in the centre of mass frame through the relative particle velocity v_{rel} at the moment of collision (Bañados, Hassanain, Silk 2011). The components of the particles' four-velocities in the reference frame of the first particle at this moment are obtained by

$$u^i_{(1)} = (1,0,0,0), \quad u^i_{(2)} = \frac{(1,\mathbf{v}_{rel})}{\sqrt{1-v^2_{rel}}}.$$ (21)

Thus, $u^i_{(1)}u_{(2)i} = 1/\sqrt{1-v^2_{rel}}$,

$$v_{rel} = \sqrt{1-\left(u^i_{(1)}u_{(2)i}\right)^{-2}}.$$ (22)

It is evident that these expressions do not depend on the coordinate system.

It follows from (20) and (22) that

$$E^2_{c.m.} = m^2_1 + m^2_2 + \frac{2m_1 m_2}{\sqrt{1-v^2_{rel}}},$$ (23)

and the unlimited growth of the collision energy in the centre of mass frame occurs due to the growth of the relative velocity to the speed of light.

For free falling particles with energies E_1 and E_2 (relative to infinity) and angular momenta J_1, J_2, the geodesic equations give

$$E^2_{c.m.} = m^2_1 + m^2_2 - \frac{2}{\rho^2}\sigma_{1\theta}\sigma_{2\theta}\sqrt{\Theta_1\Theta_2} +$$

$$+\frac{2}{\Delta\rho^2}\left[E_1 E_2 \Sigma^2 - 2Mra(E_1 J_2 + E_2 J_1) - J_1 J_2 \frac{S}{\sin^2\theta} - \sigma_{1r}\sigma_{2r}\sqrt{R_1 R_2}\right].$$ (24)

If particles move in radial coordinates in one direction ($\sigma_{1r}\sigma_{2r} = 1$), for collisions on the horizon solving the last term in (24) the indeterminacy of the form $0/0$ in the limit $r \to r_H$ gives

$$E^2_{c.m.} = m^2_1 + m^2_2 - \frac{2}{\rho^2_H}\sigma_{1\theta}\sigma_{2\theta}\sqrt{\Theta_{1H}\Theta_{2H}} + \left(m^2_1 + \frac{\Theta_{1H}}{\rho^2_H}\right)\frac{J_{2H} - J_2}{J_{1H} - J_1} +$$

$$+\left(m^2_2 + \frac{\Theta_{2H}}{\rho^2_H}\right)\frac{J_{1H} - J_1}{J_{2H} - J_2} + \frac{\rho^2_H}{4M^2 r^2_H \sin^2\theta}\frac{(J_{1H}J_2 - J_{2H}J_1)^2}{(J_{1H} - J_1)(J_{2H} - J_2)}$$ (25)

(see also (24)). Here the subscript H in ρ_H and Θ_H indicates the value of the corresponding variable on the event horizon r_H. If one of the particles has the angular momentum projection $J = J_H$ -(the critical particle) and the other particle has $J \neq J_H$, then the energy of collisions is divergent on the horizon. For extremal rotating black holes this was found by Bañados, Silk and West (2009) (the BSW effect). For nonextremal black holes in the vicinity of the horizon, $J = J_H$ is not possible; however, it is possible in case of multiple collisions (Grib, Pavlov 2010; 2011) to have J that is very close to J_H for $r \to r_H$.

For the Schwarzschild black hole $(a = 0)$, the collision energy in the centre of mass frame (Grib, Pavlov 2012) is

$$E_{c.m.}^2 (r \to r_H) = \frac{(E_1 J_2 - E_2 J_1)^2}{4M^2 E_1 E_2} + m_1^2 \left(1 + \frac{E_2}{E_1}\right) + m_2^2 \left(1 + \frac{E_1}{E_2}\right). \tag{26}$$

Here it is assumed that $\theta = \pi / 2$.

To achieve the horizon of the black hole, a massive particle falling freely into the black hole in equatorial plane with dimensionless angular momentum $A = a / M$ being nonrelativistic at infinity $(E = m)$ must have angular momentum from the interval (l_L, l_R),

$$l_L = -2\left(1 + \sqrt{1+A}\right), \quad l_R = 2\left(1 + \sqrt{1-A}\right) \tag{27}$$

(here the notation $l = J / mM$ is used). For the Schwarzschild black hole, the maximal collision energy of two free falling particles with masses $m_1 = m_2 = m$ equals $2\sqrt{5}m$ if $l_1 = \pm 4$, $l_2 = \mp 4$ (Baushev 2009).

Putting the limiting values of angular momenta l_L, l_R into the formula (25) gives the maximal collision energy values of the particles falling freely from infinity

$$\frac{E_{c.m.}^{max} (r \to r_H)}{m_1 + m_2} = \sqrt{1 + \frac{2m_1 m_2}{(m_1 + m_2)^2} \frac{(2 + \sqrt{1+A} + \sqrt{1-A})^2}{(1 + \sqrt{1-A^2})\sqrt{1-A^2}}}. \tag{28}$$

The dependence of $E_{c.m.}^{max}$ on the angular momentum of the black hole in the case $m_1 = m_2 = m$ is shown in Fig. 1.

For $A = 1 - \varepsilon$ with $\varepsilon \to 0$ the formula (28) gives

$$E_{c.m.}^{max} = 2\left(2^{1/4} + 2^{-1/4}\right) \frac{\sqrt{m_1 m_2}}{\varepsilon^{1/4}} + O(\varepsilon^{1/4}). \tag{29}$$

Therefore, even for values close to the extremal $A = 1$ of the rotating black hole, $E_{c.m.}^{max} / \sqrt{m_1 m_2}$ cannot be very large as mentioned by Berti, Cardoso, Gualtieri et al. (2009) and Jacobson and Sotiriou (2010) for the case $m_1 = m_2$. Thus, (28) for $A_{max} = 0.998$ considered as the maximal possible dimensionless angular momentum of the astrophysical black holes (Thorne 1974) gives $E_{c.m.}^{max} / \sqrt{m_1 m_2} \approx 18.97$.

However, this evaluation is enough for collisions of superheavy dark matter particles with the mass close to the grand unification scale to occur in the region of grand unification interaction physics, so that these particles can decay into quarks and be observed as the UHECR (Grib, Pavlov 2008a).

Moreover, taking into account the possibility of multiple scattering, so that the particle falling from infinity into the black hole with some fixed angular momentum changes its momentum in the result of interaction with particles in the accretion disc and then scatters again close to the horizon, then the scattering energy for usual particles can be unlimited.

The permitted interval in r for particles with $\varepsilon = 1$ and angular momentum $l = l_H - \delta$ falling in equatorial plane is obtained from (9). To do this, it is necessary to set the left side of (9) (for $dr / d\lambda$) to zero and find the root. In the second order in δ close to the horizon one has

$$l = l_H - \delta \quad \Rightarrow \quad x < x_\delta \approx x_H + \frac{\delta^2 x_C^2}{4 x_H \sqrt{1 - A^2}}. \tag{30}$$

Here $x = r / M$, $x_H = r_H / M$, $x_C = r_C / M$. The effective potential for the case $\varepsilon = 1$ defined by the right side of (9)

$$V_{eff}(x, l) = -\frac{1}{2}\left(\frac{dr}{d\tau}\right)^2 = -\frac{1}{x} + \frac{l^2}{2x^2} - \frac{(A - l)^2}{x^3} \tag{31}$$

(see, for example, Fig. 2) leads to the following behaviour of the particle. If a particle goes from infinity to the black hole, it can achieve the horizon if the inequality (27) is valid. However, the scattering energy in the centre of mass frame given by (28) is not large. On the other hand, if a particle comes not from the infinity, but from some distance

defined by (30), then, due to the form of the potential, it can have values of $l = l_H - \delta$ larger than l_R and fall into the horizon. If a particle falling from infinity with $l \le l_R$ arrives to the region defined by (30) and interacts there with other particles of the accretion disc, or decays into a lighter particle which gets an increased angular momentum $l_1 = l_H - \delta$, then the scattering energy in the centre of mass system is

$$E_{c.m.} \approx \frac{1}{\sqrt{\delta}} \sqrt{\frac{2 m_1 m_2 (l_H - l_2)}{1 - \sqrt{1 - A^2}}}, \tag{32}$$

and it increases without limit for $\delta \to 0$. For $A_{max} = 0.998$ and $l_2 = l_L$, $E_{c.m.} \approx 3.85 m / \sqrt{\delta}$. Note that for rapidly rotating black holes $A = 1 - \varepsilon$ the difference between l_H and l_R is not large

$$l_H - l_R = 2 \frac{\sqrt{1 - A}}{A}\left(\sqrt{1 - A} + \sqrt{1 + A} - A\right) \approx 2(\sqrt{2} - 1)\sqrt{\varepsilon}, \quad \varepsilon \to 0. \tag{33}$$

For $A_{max} = 0.998$, $l_H - l_R \approx 0.04$, so the possibility of getting small additional angular momentum in interaction close to the horizon seems highly probable. The probability of multiple scattering in the accretion disc depends on its particle density and is large for large densities.

Role of particles with large angular momentum

Very large energy of collisions can be obtained if, due to multiple collisions or the external field, the particle has a negative angular momentum projection with a large absolute value (Grib, Pavlov 2013a; 2013b) for the fixed value of the particle energies due to (17). As it is shown by Grib and Pavlov (2013b), for the collision in ergosphere one has

$$E_{c.m.}^2 \approx J_2 \frac{r^2 - 2rM + a^2 \cos^2\theta}{\rho^2 \Delta \sin^2\theta}\left(\sigma_{1r}\sqrt{J_{1+} - J_1} - \sigma_{2r}\sqrt{J_{1-} - J_1}\right)^2, \quad J_2 \to -\infty. \tag{34}$$

Thus, when particles fall on the rotating black hole, collisions with arbitrarily high energy in the centre of mass frame are possible at any point of the ergosphere if $J_2 \to -\infty$ and the energies E_1, E_2 are fixed. The energy of collision in the centre of mass frame is growing proportionally to $\sqrt{|J_2|}$. Note that for large $-J_2$ the collision energy close to horizon in the centre of mass frame can be either higher or lower then for collisions at the other points of ergosphere depending on values E_1, J_1.

Unbounded growth of the collision energy with growing $-J$ due to (23) is conditioned for the BSW effect by the growth of the relative velocity of particles to the speed of light. Contrary to the BSW effect, this effect can take place at any point of the ergosphere.

Outside the ergosphere, the collision energy is limited for given r, but for $r \rightarrow r_1$ it can be large if one of the particles gets an angular momentum in intermediate collisions close to J_- (see (15)). In Fig. 3 the dependence of the collision energy in the centre of mass frame in the coordinate r is shown for particles with $E_1 = E_2 = m_1 = m_2$, $J_1 = 0$ and $J_2 = J_-$ moving in the equatorial plane of a black hole with $a = 0.8M$.

Note that large negative values of the angular momentum projection are forbidden for fixed energy values of a particle out of the ergosphere. That is why collisions with $J_2 \rightarrow -\infty$ do not occur for particles falling from infinity. However, if a particle comes to the ergosphere and gets large negative values of the angular momentum projection (getting high energies is not necessary) there in the result of interactions with other particles, then its subsequent collision with the particle falling into the black hole leads to a high energy in the centre of mass frame.

Superhigh energies may be obtained in such a way from collisions of usual particles (i.e. protons); however, it is physically unrealistic. Instead, as follows from (34), the value of angular momentum necessary for getting the collision energy $E_{c.m.}$ is

$$J_2 \approx -\frac{aE_{c.m.}^2}{2E_1}. \tag{35}$$

Thus, the absolute value of the angular momentum J_2 must acquire the order $E_{c.m.}^2 / (m_1 m_2)$ relative to the maximal angular momentum value of the particle coming to ergosphere from infinity. For example, if $E_1 = E_2 = m_p$ (the proton mass), then $|J_2|$ must increase with a factor 10^{18} for $E_{c.m.} = 10^9 m_p$. It requires a very large number of collisions with getting additional negative angular momentum in each collision.

However, the situation is different for supermassive particles with mass of the grand unification scale created by gravitation in the end of the inflation era. In the ergosphere of the rotating black holes such particles can increase their energy from $2m$ to $3m$ and larger due to getting large relative velocities, so that the mechanism considered in this paper can lead to their decay, same as in the early universe. The number of intermediate collisions for them is not very large (approximately 10).

White hole geodesics

The energy of direct collisions ($\sigma_{1r}\sigma_{2r} = -1$) is divergent on the horizon

$$E_{c.m.}^2 \sim \frac{4a^2}{\Delta \rho^2}(J_{1H} - J_1)(J_{2H} - J_2) \rightarrow \infty, \quad r \rightarrow r_H, \tag{36}$$

if $J_i \neq J_{iH}$. Getting ultrahigh energy in this way is possible if one of the particles moves along white hole geodesic (Grib, Pavlov 2015a; 2015b).

Formulas (19)–(25), (34) and (36) are valid for any colliding particles with both positive and negative (relative to infinity) energy. For any value of the particle energies, the energy in the centre of mass frame satisfies the inequality

$$E_{c.m.} \geq m_1 + m_2, \tag{37}$$

because colliding particles in the centre of mass frame are moving one to another with certain velocities. All three ways of getting infinitely high energy from collisions are also possible for particles with negative (zero) energy.

The physical importance of these resonances is due to possible conversion of dark matter particles into visible ones in the ergosphere of astrophysical black holes (Grib, Pavlov 2008a; 2009).

Some calculations of the collision energy for two particles with equal masses m, one of which falls from the infinity into a black hole and another one has positive, zero or negative energy, and their results are presented in the paper by Grib and Pavlov (2017).
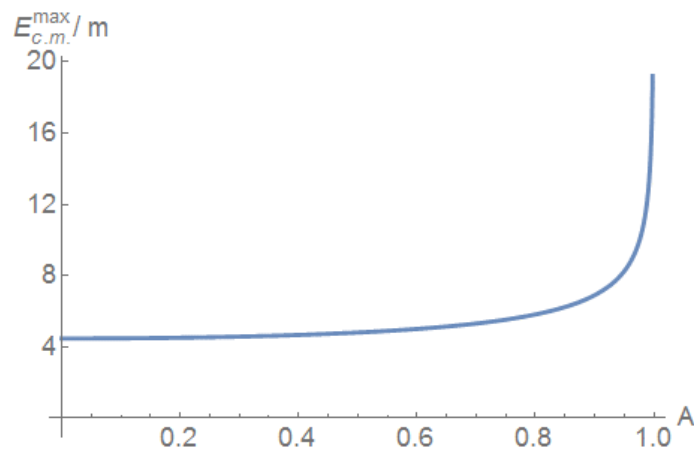
Fig. 1. The dependence of the maximal energy of collision for particles falling from infinity on the black hole angular momentum
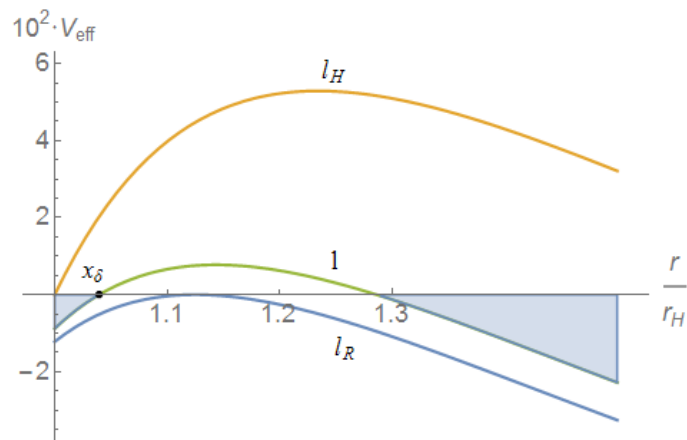

Fig. 2. The effective potential for $A = 0.96$ and $l_R = 2.4$, $l = 2.44$, $l_H \approx 2.67$. Allowed zones for $l = 2.44$ are shown by the gray color
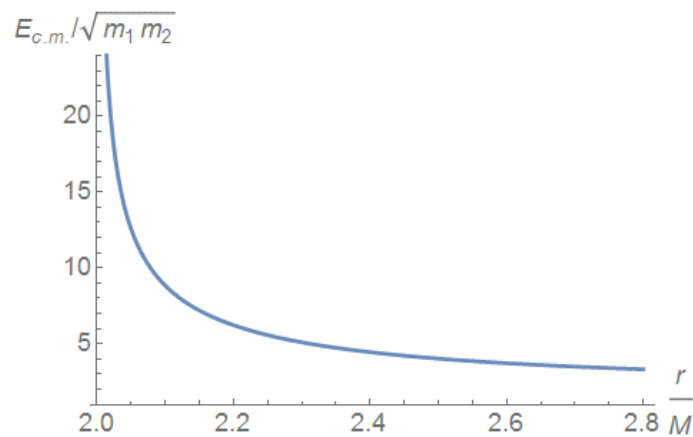

Fig. 3. The collision energy in the centre of mass frame for particles with $J_1 = 0$ and $J_2 = J_-$ out of the ergosphere

Conclusion

1. Energies of the grand unification and Planck scale in the centre of mass frame for two colliding particles can be obtained in the horizon vicinity of the Kerr nonextremal black hole, if one particle gets the critical angular momentum in previous multiple collisions.

2. Such energies can be obtained at any point of the ergosphere, if one of the particles has a negative angular momentum with a large absolute value.

3. "White hole" geodesics exist in the vicinity of black holes. They can be positive energy geodesics and Penrose geodesics with negative energies in the ergosphere. Particles on these geodesics can collide with ordinary particles and high energy can be obtained either in direct collisions or in case of large negative angular momentum of one of the particles.

4. The hypothesis of superheavy dark matter particles with grand unification mass which decayed partially into ordinary particles in the early universe, giving the observable Eddington number at the time close to the era of particle creation from vacuum, can be examined in the vicinity of Kerr black hole.

References

Aab, A., Abreu, P., Aglietta M. et al. (2017) Observation of a large-scale anisotropy in the arrival directions of cosmic rays above 8×10^{18} eV. *Science*, 357 (6357), 1266–1270. DOI: 10.1126/science.aan4338 (In English)

Bañados, M., Hassanain, B., Silk, J., West, S. M. (2011) Emergent flux from particle collisions near a Kerr black hole. *Physical Review D*, 83 (2), 023004. DOI: 10.1103/PhysRevD.83.023004 (In English)

Bañados, M., Silk, J., West, S. M. (2009) Kerr black holes as particle accelerators to arbitrarily high energy. *Physical Review Letters*, 103 (11), 111102. DOI: 10.1103/PhysRevLett.103.111102 (In English)

Baushev, A. (2009) Dark matter annihilation in the gravitational field of a black hole. *International Journal of Modern Physics D*, 18 (08), 1195–1203. DOI: 10.1142/S0218271809014509 (In English)

Berti, E., Cardoso, V., Gualtieri, L. et al. (2009) Comment on "Kerr black holes as particle accelerators to arbitrarily high energy". *Physical Review Letters*, 103 (23), 239001. DOI: 10.1103/PhysRevLett.103.239001 (In English)

Boyer, R. H., Lindquist, R. W. (1967) Maximal analytic extension of the Kerr metric. *Journal of Mathematical Physics*, 8 (2), 265–281. DOI: 10.1063/1.1705193 (In English)

Chandrasekhar, S. (1983) *The mathematical theory of black holes.* Oxford: Clarendon Press, 646 p. (In English)

Frolov, V. P., Novikov, I. D. (2012) *Black hole physics: Basic concepts and new developments.* S. l.: Springer Science & Business Media, 770 p. DOI: 10.1007/978-94-011-5139-9 (In English)

Grib, A. A., Mamayev, S. G., Mostepanenko, V. M. (1994) *Vacuum quantum effects in strong fields.* Saint Petersburg: Friedmann Laboratory Publ., 361 p. (In English)

Grib, A. A., Pavlov, Y. V. (2002a) Cold dark matter and primordial superheavy particles. *International Journal of Modern Physics A*, 17 (29), 4435–4439. DOI: 10.1142/S0217751X02013514 (In English)

Grib, A. A., Pavlov, Yu. V. (2002b) Superheavy particles in Friedmann cosmology and the dark matter problem. *International Journal of Modern Physics D*, 11 (03), 433–436. DOI: 10.1142/S0218271802001706 (In English)

Grib, A. A., Pavlov, Yu. V. (2008a) Do active galactic nuclei convert dark matter into visible particles? *Modern Physics Letters A*, 23 (16), 1151–1159. DOI: 10.1142/S0217732308027072 (In English)

Grib, A. A., Pavlov, Yu. V. (2008b) Is dark matter the relic of the primordial matter that created the visible matter of the universe? *Gravitation and Cosmology*, 14 (1), 1–7. DOI: 10.1134/S0202289308010015 (In English)

Grib, A. A., Pavlov, Yu. V. (2009) Active galactic nuclei and transformation of dark matter into visible matter. *Gravitation and Cosmology*, 15 (1), 44–48. DOI: 10.1134/S0202289309010125 (In English)

Grib, A. A., Pavlov, Yu. V. (2010) On the collisions between particles in the vicinity of rotating black holes. *JETP Letters*, 92 (3), 125–129. DOI: 10.1134/S0021364010150014 (In English)

Grib, A. A., Pavlov, Yu. V. (2011) On particle collisions in the gravitational field of the Kerr black hole. *Astroparticle Physics*, 34 (7), 581–586. DOI: 10.1016/j.astropartphys.2010.12.005 (In English)

Grib, A. A., Pavlov, Yu. V. (2013a) On the energy of particle collisions in the ergosphere of the rotating black holes. *EPL (Europhysics Letters)*, 101 (2), 20004. DOI: 10.1209/0295-5075/101/20004 (In English)

Grib, A. A., Pavlov, Yu. V. (2013b) Collision energy of particles in the ergosphere of rotating black holes. *Theoretical and Mathematical Physics*, 176 (1), 881–887. DOI: 10.1007/s11232-013-0075-4 (In English)

Grib, A. A., Pavlov, Yu. V. (2015a) Are black holes totally black? *Gravitation and Cosmology*, 21 (1), 13–18. DOI: 10.1134/S0202289315010065 (In English)

Grib, A. A., Pavlov, Yu. V. (2015b) High energy physics in the vicinity of rotating black holes. *Theoretical and Mathematical Physics*, 185 (1), 1425–1432. DOI: 10.1007/s11232-015-0351-6 (In English)

Grib, A. A., Pavlov, Yu. V. (2017) Black holes and particles with zero or negative energy. *Theoretical and Mathematical Physics*, 190 (2), 268–278. DOI: 10.1134/S0040577917020088 (In English)

Grib, A. A., Pavlov, Yu. V., Piattella, O. F. (2012) On collisions with unlimited energies in the vicinity of Kerr and Schwarzschild black hole horizons. *Gravitation and Cosmology*, 18 (1), 70–75. DOI: 10.1134/S0202289312010094 (In English)

Harada, T., Kimura, M. (2011) Collision of two general geodesic particles around a Kerr black hole. *Physical Review D*, 83 (8), 084041. DOI: 10.1103/PhysRevD.83.084041 (In English)

Jacobson, T., Sotiriou, T. P. (2010) Spinning black holes as particle accelerators. *Physical Review Letters*, 104 (2), 021101. DOI: 10.1103/PhysRevLett.104.021101 (In English)

Kerr, R. P. (1963) Gravitational field of a spinning mass as an example of algebraically special metrics. *Physical Review Letters*, 11 (5), 237. DOI: 10.1103/PhysRevLett.11.237 (In English)

Misner, C. W., Thorne, K. S., Wheeler J. A. (1973) *Gravitation*. San Francisco: W. H. Freeman & Company, XXVI, [2], 1279 p. (In English)

Piran, T., Shaham, J., Katz, J. (1975) High efficiency of the Penrose mechanism for particle collisions. *Astrophysical Journal Letters*, 196, L107. DOI: 10.1086/181755 (In English)

Thorne, K. S. (1974) Disk-accretion onto a black hole. II. Evolution of the hole. *Astrophysical Journal*, 191, 507–520. DOI: 10.1086/152991 (In English)

Zaslavskii, O. B. (2013) Acceleration of particles as a universal property of ergosphere. *Modern Physics Letters A*, 28 (11), 1350037. DOI: 10.1142/S0217732313500375 (In English)